Characterization of fluid flow in paper-based microfluidic devices

by

Noosheen Walji

A Thesis Submitted in Partial Fulfillment of the
Requirements for the Degree of

Master of Applied Science

in

The Faculty of Engineering and Applied Science

Mechanical Engineering

University of Ontario Institute of Technology

July 2015

Table of Contents

Abstract

Paper-based microfluidic devices are being leveraged for application of diagnostic and detection technology in low-resource settings. In order to design a highly accurate device, a mathematical model is required to predict flow behaviour in the paper-based microfluidic devices. A series of experiments were conducted to observe the parameters that influence fluid flow behaviour in paper during imbibition. The parameters investigated included temperature, humidity, machine direction, length, and width. Experiment results showed that variations in fluid temperature and width of the paper device influenced wicking time, and a post-wetting flow was also observed. Two common modelling methods, the Washburn equation and Darcy's law, were evaluated to determine the most appropriate method for predicting flow behaviour in paper. A mathematical model was developed along with an empirically determined expression for permeability.

Acknowledgements

I would like to thank my supervisor, Dr. Brendan MacDonald, for his unwavering support. Brendan's enthusiasm and knowledge have created a rich learning environment that has been a privilege to be part of. I am immensely grateful for his guidance through academic and personal matters, which has enabled me to grow beyond what I thought myself capable of. Thank you for teaching me to approach challenges with curiosity and confidence, and for encouraging me to pursue my passion.

Many thanks to my lab mates for the insightful conversations and for keeping a smile on my face. A special thank you to Mostasim Mahmud, whose wisdom and kindness taught me invaluable lessons about academia, but more importantly about life and its many beauties. I would also like to thank Mostasim's family for their hospitality during our time in Bangladesh. Thank you to my colleague and good friend, Ofelia Jianu, for the much needed moral support and comradery. To my friends, I extend a heartfelt thank you for your companionship. A big thank you to Mandy Pieroni, whose compassion and optimism carried me through. Thanks to Crystal Ramchandani, for the countless words of encouragement every step of the way, and for taking the time to read through my work. Also, thank you to Korryn Bodner for keeping me focused while simultaneously helping me push the boundaries of what it is to be normal.

I would also like to thank my family for their unconditional love and support. Thank you to Irfan, Tiffany, and Darcy for being a shoulder to lean on. A special thank you to my mom, Bilkis Walji, for teaching me what it means to be resilient. She has been an incredible role model, her patience and understanding have helped me build a life I am proud of.

List of Tables

List of Figures

Nomenclature

a_c	cross-sectional area (m^2)
g	gravitational acceleration ($m\ s^{-2}$)
h_l	height of liquid in capillary (m)
h	thickness of paper (m)
P_E	total external pressure (Pa)
P_c	capillary pressure (Pa)
∇P	pressure gradient ()
P	pressure (Pa)
P_A	atmospheric pressure (Pa)
r_c	capillary radius (m)
r_{eff}	effective pore radius (m)
t	time (s)
v	fluid velocity ($m\ s^{-1}$)
V	volume (m^3)
x	position of fluid front (m)
γ	surface tension at the liquid-gas interface ($N\ m^{-1}$)
ϵ	coefficient of slip
θ	contact angle (^{o})
κ	permeability (m^2)
κ'	degree of penetration ($m^{1/2}\ s^{-1}$)
μ	dynamic viscosity (Pa s)
ρ	density ($g\ m^{-3}$)
ρ_{BW}	basis weight of paper ($g\ m^{-2}$)
ρ_c	density of cellulose ($g\ m^{-3}$)
ϕ	porosity of paper

Chapter 1

Introduction

1.1 Motivation

Access to clean drinking water is a key factor in improving health and the quality of life on a global scale, particularly in low-resource areas where centralized water monitoring systems have not yet been established. A recent report on the status of water supply and sanitation by the World Health Organization approximates about 780 million people do not have access to clean water, resulting in 3.4 million deaths each year [1], [2]. In 2000, the United Nations identified "sustainable access to safe drinking water" as one of the Millennium Development Goals to eradicate poverty and improve well-being [3]. While substantial progress has been made to expand accessible water sources by several NGOs, there remains the issue of sustaining these sources [4]. Regular and affordable water testing services has been identified as an essential factor to establish sustainable access to clean water [5]. In the case of developing communities, especially those with high population density, the lack of water management infrastructure and financial resources have created a critical need for low-cost, accessible water monitoring technology.

Arsenic groundwater contamination in Bangladesh has been referred to as the greatest environmental disaster in history and a public health emergency by the World Health Organization

(WHO) [6]. Due to high levels of anthropogenic and natural pollution in the surface waters, the main source of water in Bangladesh is the groundwater, which is pumped to the surface using tube wells. In the 1970s, UNICEF partnered with the Department of Public Health Engineering in Bangladesh to install tube wells around the country in an effort to improve access to water [6]. Arsenic-related illnesses were first detected in the 1980s, and the extent of the large scale, naturally occurring arsenic contamination in the groundwater was established by 1998 [6], [7]. WHO has identified that 1 in 5 people are at risk of exposure to arsenic contamination [6], [8]. The most common implications of exposure to arsenic contaminated water, both acute and chronic, are skin lesions and cancers [9], however, arsenic can have damaging effects to physiological systems throughout the body [10], [11]. UNICEF continued to work with the Bangladesh government in the 2000s to test the tube wells for arsenic using a field test kit, the safety of the tube well was then indicated by painting it red for contaminated, or green for safe [12]. While this initiative was effective in quantifying the contamination problem and educating citizens, it has not provided a long-term monitoring system. Geological studies on the groundwater in Bangladesh have suggested that the arsenic concentration has not yet reached steady state in the groundwater, and is therefore susceptible to large fluctuations over time [13]. This contamination continues to be a serious and widespread issue in Bangladesh. Efforts from the government and partnering NGOs have made significant advances to improving access to water, however, resources for regular and affordable water contamination testing have become crucial to mitigating the arsenic contamination problem and facilitating the management of water sources.

Current commercially available arsenic field test kits, similar to those utilized by UNICEF, are difficult to use, involve potentially harmful chemicals, and provide inconsistent results. These test kits are based on a mercury bromide stain method of arsenic detection, where reagents are added to water to release arsenic in the form of arsine gas, which then reacts with a mercury

bromide paper. A colour change occurs on the mercury bromide paper, and the intensity of the resulting colour is used to determine the arsenic concentration in the water sample by comparison to the colour card provided. This multi-step method introduces multiple opportunities for human error, and the colour change can be difficult to distinguish to the untrained eye. Additionally, both the mercury bromide and the arsine gas are highly toxic substances that can be hazardous if mishandled [14]–[17]. In a comparative study by Pande et al., five mercury bromide stain arsenic test kits were evaluated and found incapable of detecting arsenic concentrations near the WHO water safety limit of 10 μg/L [18]. A more recent investigation by Rahman et al. in Bangladesh found that 45% of the tube wells they tested were mislabelled [14]. Jakariya et al. also conducted a study to compare the results of a field test kit to laboratory measurements using atomic absorption spectrometry, demonstrating that field kit was incorrect for 9% of tube well samples compared to the Bangladesh water safety limit of 50 μg/L and 13% compared to the WHO limit of 10 μg/L [16]. An appropriate tool is needed that is user-friendly, safe, and reliable for detection of arsenic at the safety limit of 10 μg/L.

Microfluidic devices have become a research area of interest for the application of detection and diagnostic processes in low-resource areas. Microfluidic technology is referred to as the miniaturization of reaction, separation, detection, and diagnostic processes [19]. Microfluidic devices typically include a network of microchannels where fluids are transported and processed, and are often produced on the silicone-based polymer, PDMS [20]. The effectiveness of microfluidic devices in low-resource areas has prompted the World Health Organization to establish guidelines for developing microfluidic diagnostic devices. These guidelines are referred to as the ASSURED principles, indicating that microfluidic devices should aim to be Affordable, Sensitive, Specific, User-friendly, Rapid and robust, Equipment-free, and Deliverable to end users [21], [22]. Here sensitivity is defined as avoiding false negative results, and specificity refers to

avoiding false positive results [22]. According to these guidelines, paper is inherently advantageous as a platform for microfluidic devices. Not only is it an affordable and accessible material, the wicking mechanism in paper allows for the passive transport of fluids, eliminating the need for auxiliary equipment. Paper as a material is easy to stack, package, and store since it lays flat. Specificity and selectivity can be enabled with chemical reactions pre-programmed onto the paper, which involves selecting the geometry of the paper and the placement of the reagents to control the reaction as the fluid wicks through the paper. Paper-based microfluidic devices are typically user-friendly, as they eliminate the need for sample treatment or fluid manipulation, and can provide a simple colorimetric signal readout. Rapidness and robustness will depend on the design details, such as reaction chemistry and the physical design of the device. Paper offers the additional benefit of being compatible with a variety of chemicals and biomaterials, as well as chemical treatments such as nitration. In this way, paper is an ideal platform for microfluidics and provides versatility in its physical and chemical flexibility.

In order to design an ASSURED paper-based assay for arsenic, a mathematical model is required to accurately predict flow behaviour in the paper such that reagents can be placed accordingly. Mathematical models based on the well-established Washburn equation for capillary flow or Darcy's law for flow in porous media have been developed to predict fluid flow behaviour in paper. The structure of paper on the microscale is complex, as it is classified as a porous medium as well as a fibrous medium, and the fluid transport mechanism has been identified as capillary-driven flow. Since the structure of the fibrous matrix in paper is highly complex, simplifying approximations are made at the expense of accuracy and precision. To apply the Washburn equation, the paper fibre structure is approximated as a bundle of capillaries created by an alignment of pores. However, this assumption is challenged by the ambiguity around selecting a representative pore size as the capillary radius. Furthermore, an investigation on permeability of

paper by Rasi clarifies that the fibre structure of paper includes both interfibre pores and intrafibre pores [23]. With this observation, it becomes counter-intuitive to assume that pores in paper would form continuous capillaries for fluid to flow through, compounded with the additional complication of identifying an appropriate representation for capillary size when such a large pore size distribution exists. Additionally, the influence of paper fibre effects, such as swelling and deformation, are not addressed in this model. Though the presence of capillary forces are addressed in the Washburn model, it is challenging to determine an appropriate capillary size and resistances caused by the fibrous network are not addressed. While experimental studies for imbibition in paper have been unable to generate accurate predictions using the Washburn equation [24]–[26], other studies have seen more success in applying Darcy's law where the fluid flow is driven by a pressure gradient to permeate through a porous medium [27]–[31]. Here the concept of permeability attempts to encompass some of the complexities of flow through the fibrous paper network. Since permeability is an empirically determined parameter, it provides the versatility to incorporate a variety of parameters as an understanding of their impacts are developed. As such, a working model for fluid flow through paper-based microfluidic devices has yet to be established, but can be developed once a deeper understanding is acquired of the parameters that influence fluid flow in paper-based microfluidic devices.

In summary, the motivation for this thesis is the need for an understanding of fluid flow through paper to assist in the design and application of a reliable paper-based arsenic detection device in Bangladesh. The findings of this thesis can then be expanded for paper-based microfluidic devices in a variety of applications.

1.2 Microfluidic Paper-Based Analytical Devices

Microfluidic paper-based analytical devices (μPADs) have shown promise for point-of-interest testing, which refers to testing at the location where information is required rather than in a laboratory. In this section, recent developments in paper-based microfluidics are summarized to observe how existing μPADs are applied, and to gain an understanding of the possible conditions or parameters that need to be addressed in a mathematical model that aims to predict flow behaviour in such devices.

Many notable applications of paper-based microfluidics have been in the context of diagnostics and environmental testing in low-resource settings. For example, Chin et al. integrated an ELISA on paper to diagnose HIV and syphilis in microliter volumes of unprocessed blood samples. Application in the field was demonstrated successfully in Rwanda, with interest from healthcare workers in India and Tanzania [32]. Similarly, Gong et al miniaturized a hepatitis B detection test encased in a pen format for safe sample containment, with successful clinical application in Vietnam [33]. Devices have also been fabricated for contamination detection in food and water, such as salmonella and heavy metals [34], [35]. In each μPAD design, a key concern is achieving an appropriate detection sensitivity and selectivity to avoid false results. These innovations in μPAD designs are indicative of the potential for paper-based technology to have an immense positive impact on the global society by increasing access to health care as well as clean food and water. A vital consideration in the successful application of this technology on a global scale are the climate zones they are applied in. In the aforementioned studies, Rwanda has a tropical highland climate with temperatures ranging from 15^{o}C to 30^{o}C and a humidity range of 38% to 100%, and Vietnam experiences tropical climates with temperatures between 20^{o}C and 35^{o}C and humidity between 50% and 98%. In Bangladesh the climate zone is described as a tropical savannah, with temperatures varying from 15^{o}C to 40^{o}C, and humidity from 25% to 95%.

In devices where the consistency of results in each test is necessary regardless of the point-of-interest location, a detailed understanding of the influence of temperature and humidity is beneficial to the design process. Therefore, a mathematical model intended to aid the design process for highly impactful μPADs should be able to address variations in ambient conditions.

Recent developments have rapidly increased the analytical capacity and complexity of microfluidic paper-based analytical devices (μPADs) through structural enhancements and flow control techniques. Fabrications strategies have grown to include two- and three-dimensional paper-devices [36], [37], with fluid manipulation elements such as pumps [38] and valves [39]. Moreover, paper devices have been designed to facilitate multi-step chemistry [40] and analyte transport after wetting [41]. These features have significantly expanded the number of constituents that can be analyzed using μPADs, which is paralleled by a growing demand for highly sensitive and specific devices. Paper device structure enhancements can be fine-tuned for predictable flow behaviour with a mathematical model that encompasses the impacts of various physical design parameters such as the shape and size of the paper. Therefore, a deeper understanding of the influence of shape and size parameters of paper would benefit the design process for μPADs.

In summary, recent developments in structural features of μPADs, and the applications for low-resource areas have demonstrated opportunities where a mathematical model that can effectively predict fluid flow behaviour through paper devices would benefit the μPAD design process. A successful mathematical model will address the impacts of ambient conditions, such as temperature and humidity, as well as the physical shape and size parameters of the paper.

1.3 Modelling of Capillary-Driven Flows

The passive wicking mechanism in paper is caused by capillary forces between the liquid and the fibres in the paper, and is referred to as capillary-driven flow. In this section, a mathematical model

for capillary-driven flow and its applications to paper media are summarized in order to investigate the existing approaches to predict capillary-driven fluid flow through paper.

Capillary-driven flow is fluid flow mechanism driven by a capillary pressure, which is the pressure gradient that occurs across the fluid meniscus in a capillary due to surface tension forces created by molecular cohesion within the fluid. These molecular cohesion forces create a curvature at the liquid-air interface, characterized by a contact angle. The contact angle describes the angle between the solid-liquid interface, and the liquid-air interface. A wetting fluid will typically have a contact angle below 90°, resulting in a concave curvature, while a non-wetting fluid will have a contact angle above 90°, and subsequently a convex curvature, as demonstrated in Figure 1.

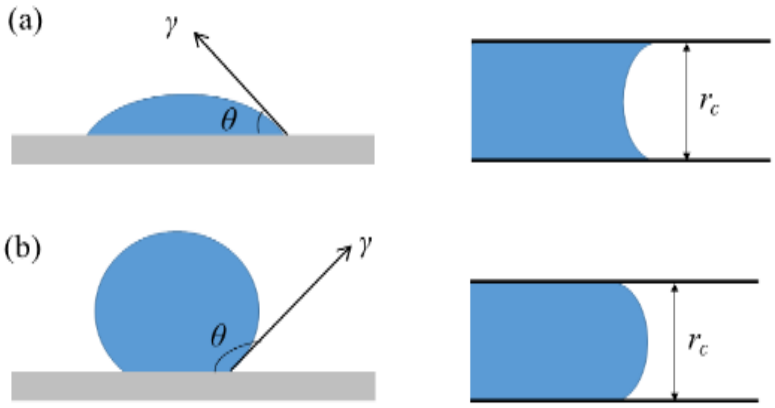

Figure 1. Contact angle and liquid-air interface shape in a capillary for (a) wetting fluids and (b) non-wetting fluids.

Where there is a non-zero surface tension across a curved fluid surface, a pressure drop exists across the interface [42], [43]. The capillary pressure of a fluid can be described using the Young-Laplace equation (Equation 1), which is a function of surface tension (γ) and contact angle (θ), as

$$P_c = \frac{2\gamma \cos\theta}{r_c} \tag{1}$$

well as capillary size (r_c). It is derived from a Gibbs free energy balance at the interface at equilibrium, or quasi-equilibrium, where surface energy is balanced by the pressure-volume energy [42], [44], [45]. The Young-Laplace equation can be applied to paper if the surface tension of the liquid and its contact angle with the paper fibre material is known. However, capillary size parameter for paper remains an ambiguous term, as it is difficult to quantify for the fibre structure of paper.

Capillary-driven flows are typically modelled using the Washburn equation (Equation 2)

$$x^2 = \frac{\gamma \cos\theta}{2\mu} r_c t, \tag{2}$$

developed by Edward Washburn in 1921. The Washburn equation is derived using Poiseuille's law for pressure driven flow in a cylinder with no slip. The pressure term in Poiseuille's equation is expressed using the Young-Laplace equation for capillary pressure. The capillary is assumed to be open at both ends, and gravitational forces are assumed to be negligible, therefore, both atmospheric and hydrostatic pressures are deemed negligible [46]. Washburn also suggested that the rate of penetration of a porous body by a liquid can be taken as equivalent to the rate of penetration of *n* cylindrical capillary tubes, where the volume penetrated is proportional to time using a degree of penetration parameter, similar in concept to permeability. The Washburn equation indicates that the viscosity and surface tension of the liquid, its contact angle with the paper fiber material, and the capillary size are the key parameters that influence fluid flow in paper. Once again, the application of this model to paper media is hindered by the uncertainty of the capillary size term.

Studies have investigated modifications of the Washburn equation in an attempt to address the complexities of the paper fibre structure. Schuchardt et al. adapted the Washburn equation for

swelling porous media using a hydraulic radius, which decreased with time behind flow front due to swelling of fibres, in place of capillary radius and applied a correction term that is a ratio of a swelling effect constant and the initial hydraulic pore radius. Using the properties of water, an initial pore size of 0.88 μm, and a pore radius reduction rate of 8.4×10^{-10} s^{-1}, the study found that the model matched the experimental results for wicking of water using a composite paper (cellulose and 13% FC CMC) [24]. While investigating details of the wicking mechanism for fluid in paper, Roberts et al. applied the Washburn equation to predict flow to find that Washburn predictions overestimated wicking distance by orders of magnitude. This corresponded with Roberts' observation that the fluid is more likely to flow along channels created by adjacent fibres rather than capillaries formed by aligned pores. Washburn himself had stated that the equation would not be applicable if the pores cannot be taken as cylindrical pores. Roberts adapted the Washburn equation for channel flow along a crevice, building on work by Lenormand et al. who approximated hydraulic diameter for wetting fluid at a sharp corner. The resulting model gave a closer approximation for wicking distance, but was found to consistently overestimate by a factor of 2 or 3. This was thought to be due to the hydraulic diameter approximation not addressing the many different crevice angles, as it only considered a sharp or 90^{o} corner [25], [46], [47]. In a recent study of μPAD design, Songok et al. applied the Washburn equation to describe fluid flow in a paper channel with hydrophobic barriers, however, all variables except for time were compounded into an empirical constant that fit the data and was later used for comparison between different types of liquids [48].

In summary, there seems to be a common uncertainty in the most effective way to apply the Washburn equation to a paper medium, as the idea of a bundle of capillaries only loosely relates to the fibre network structure in paper and an estimation of capillary size or an empirical fit was required. Additionally, the concepts of fibre swelling and wicking along fibres were incorporated

in the Washburn model to obtain a more appropriate representation of flow behaviour in paper, indicating that fibre behaviour plays a key role in the transportation of fluids through paper. Despite addressing fibre behaviour, estimations and empirical fits for the ambiguous capillary size parameter for paper were required. These findings were specific to the types of paper used in the studies, and are not applicable to the pure cellulose chromatography papers utilized in experiments for this thesis.

1.4 Modelling Flow Through Porous Media

The complex fibre network structure of paper is referred to as a porous medium, where the void spaces between the fibres act as pores. In this section, a mathematical model for flow through porous media and its applications to paper media are summarized in order to investigate the existing approaches to predict fluid behaviour in paper.

Porous media flows are described using Darcy's law (Equation 3), which relates fluid flow (v) with

$$v = -\frac{\kappa}{\mu}\nabla P \tag{3}$$

permeability (κ), viscosity (μ), and a pressure gradient (∇P). Darcy's law was determined empirically in 1856 for application to the flow of water through sand and dirt [49]. Since then, theoretical derivations of Darcy's law using the Navier-Stokes equation have been explored [50]. Unlike the Washburn equation, Darcy's law does not prescribe a specific geometry to the paper fiber network, and the permeability term provides a versatile and robust element that can describe several different types of porous media.

Darcy's law was recently investigated for its application to paper-like media by Masoodi et al., who proposes an adaption to the model that addresses the fibre swelling effects in paper. Here, a sink term is applied to the continuity equation to account for absorption of fluid by the

fibres, and an expression for decreasing pore size is determined to describe fibre swelling. These adjustments are applied to Darcy's law, as well as several models for permeability in porous and fibrous media. Each of the permeability models Masoodi investigated included an arbitrary constant to describe the porous media structure. When the permeability models were modified to address fibre swelling and subsequent changes in porosity, an approximated value for initial permeability of the medium (prior to any swelling effects) was applied. Both the arbitrary constant and the approximated initial permeability add an element of ambiguity to the application of Darcy's law to fluid flow in paper-based microfluidic devices [28].

In a numerical approach using COMSOL, Mendez et al. applied Darcy's law to model flow behaviour in μPADs that were straight channels connected to a fan-shaped section. Flow behaviour at the fluid front and in the straight channel were monitored to determine the impacts of downstream geometry on upstream flows within the paper. They conclude that a quasi-steady flow can be achieved in the fan portion of the paper without the use of an absorbent pad [29]. Similarly, Fu et al. applies Darcy's law with an assumed permeability value for paper to explore fluid flow in channels where the width increases or decreases after an initial wicking section. Fluid behaviour is investigated analytically, experimentally, and through computation simulations. Analytical expressions are set-up using an electrical circuit analogy where each section of a different width is one resistor, and these predictions were consistent with both experimental and simulated results [31]. Paper geometry was further inspected by Elizalde et al., who looked at fluid flow through paper strips with increasing or decreasing cross sectional area. An analytical model was developed based on Darcy's law, to describe fluid flow as a function of cross sectional area as well as a diffusive coefficient that incorporated permeability, where permeability was represented using a simplified capillary-based model. The model was found to correlate well with experimental data [51].

The permeability term in Darcy's law describes the medium's ability to transport fluids through it. Though this qualitative definition is widely accepted, permeability is typically quantified empirically or semi-empirically and varies with the type of porous medium. A commonly-used basis for permeability models is the Kozeny-Carman expression, based on porosity, specific surface area within the medium (i.e. of each fibre in the medium), and an empirical shape factor. Koponen et al. adapt this expression for random fibre webs in a simulation-based investigation to find that permeability depends exponentially on porosity, with the unique contribution of expressing the typically empirical shape factor as a function of porosity [52]. Dullien outlines several adaptions of the Kozeny-Carman equation to express permeability for different types of porous media, most of which were functions of porosity, pore size, and sometimes tortuosity [53]. More recently, Rasi conducted a study specifically on the permeability of different types of paper, and found empirical fits for a generalized form of the Kozeny-Carman equation [23]. These studies demonstrate the robustness of the permeability parameter in the sense that it can incorporate a variety of variables that are deemed significant to flow in a specific porous medium. For paper-based microfluidic devices, an expression for permeability has not yet been established. As an investigation of the parameters that influence flow behaviour in paper-based microfluidic devices is conducted, parameters that are found to have significant impact on flow behaviour can be used to build an expression for permeability.

In summary, Darcy's law has shown promise in its ability to predict flow behaviour through different types and geometries of paper, typically with some approximation or assumption to determine the pore size or permeability. A common approximation, model, or method for determining permeability has not yet been established for the design of paper-based microfluidic devices. An expression for permeability can be developed once the parameters significant to fluid flow are experimentally identified. A successfully developed expression for permeability can then

be applied in Darcy's law to predict flow behaviour in paper, and utilized as a design tool for the fabrication of a paper-based arsenic detection device.

1.5 Parameters

Fluid flow in paper-based microfluidic devices may be impacted by several physical and chemical parameters related to the liquid properties, paper properties, and surrounding conditions. In the context of μPADs for low-resource areas, the impact of temperature and humidity on fluid flow through paper needs to be investigated. In particular, the possible climate conditions in Bangladesh should be investigated, where temperatures vary from 15°C to 40°C and humidity ranges from 25% to 95%. Additional parameters of interest are paper geometry. For the simplest case of a rectangular paper strip of uniform width, the impacts of thickness, width, and length of the strip should be explored. Experimental observations and analysis of the influence of these parameters will provide a foundation for the development of a mathematical model that can accurately predict flow behaviour in a paper-based microfluidic device. Parameters that demonstrate a significant impact on flow behaviour will be built into an expression for permeability to be applied with Darcy's law.

1.6 Scope of Thesis

To design a reliable and highly effective paper-based arsenic detection device, a mathematical model is needed to predict fluid flow behaviour in paper. Paper is a complex medium due to its fibre network structure, and the parameters that influence flow through this fibrous medium are not well understood. Considering these points, this thesis has two main objectives:

- To develop a comprehensive understanding of the parameters that influence flow behaviour in a paper-based microfluidic device through experimentation, with an

emphasis on the impact of ambient conditions and easy-to-modify variables such as length, width, and machine direction.

- To develop a mathematical model that accurately describes fluid flow behaviour in paper-based microfluidic devices using appropriate and measurable variables, and determine an expression for permeability that includes the parameters investigated experimentally.

Chapter 2

Experimental Methods

The purpose of this thesis is to understand the influence of several physical properties during imbibition of paper, such as the paper geometry and the surrounding conditions. Characterizing fluid flow through paper is challenging because paper is a complex medium, however, an understanding of the parameters that influence fluid flow in paper will enhance its application as a platform for analytical chemistry in paper-based microfluidic devices. Parameters of interest are the temperature and humidity, because paper-based microfluidic devices are intended for use in low-resource areas that can be located in a variety of climate zones. Paper geometry is also of interest to determine the variables that can be used to manipulate the fluid flow in the device, and the variables that offer design flexibility. This thesis seeks to experimentally observe the behaviour of paper and fluids during imbibition of a paper strip.

2.1 Apparatus Overview

The experimental apparatus used in this study is shown in Figure 2. It consists of a temperature and humidity controlled chamber, a fluid reservoir, and a camera.

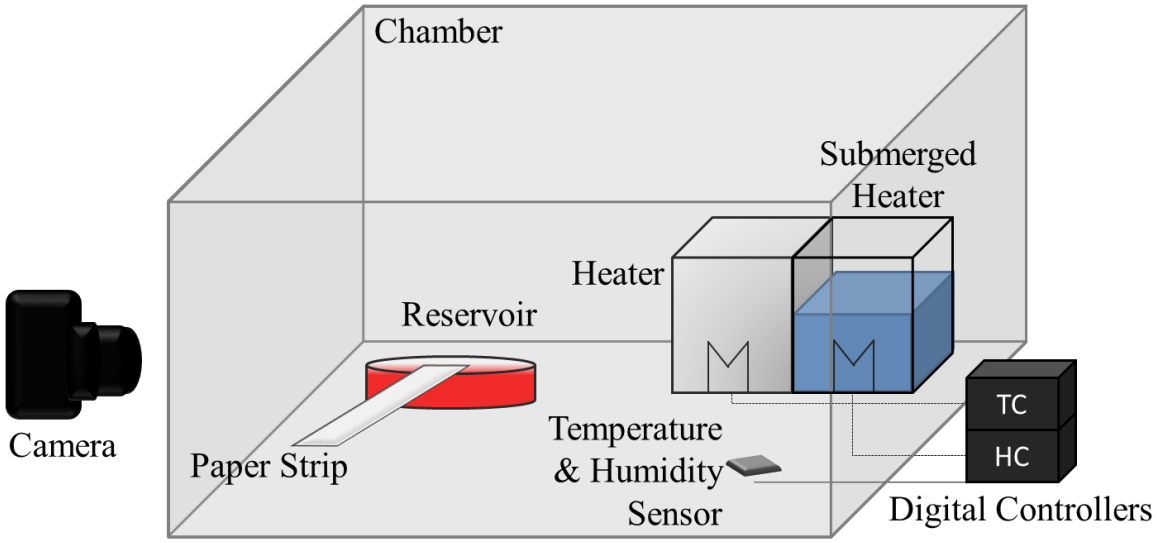

Figure 2. Schematic of experimental apparatus

A chamber 51.5 cm in width, 41.5 cm in height, and 41 cm in depth was built using an aluminum frame and transparent acrylic panels. An acrylic panel door was installed onto the chamber using standard hinges. The panel door was sealed using a foam lining around the perimeter of the panel to prevent heat transfer, while bolts with wing nuts were used to fasten the door closed during experiments. During experimentation at high temperatures, the acrylic panels were insulated with reflective aluminum bubble foil.

The temperature inside the chamber was controlled using an AGPtek STC-1000 digital controller placed outside the chamber. The controller received temperature readings from a digital thermometer inside the chamber and relayed a signal to the heater inside the chamber. A 250 W heat lamp was used as the heater, with an aluminum shade to prevent any interference from radiation. Similarly, humidity was controlled using an AGPtek WH8040 digital controller placed outside the chamber. The controller received temperature and humidity readings from a digital thermometer and hygrometer inside the chamber and relayed a signal to a humidifier inside the

chamber. The humidifier was composed of an open reservoir of water with a 7.5 W submerged heater.

The fluid reservoir was contained in a 10 cm diameter petri dish inside the chamber. The petri dish was filled with water dyed with 12.5 mmol concentration of Allura red food colour dye to a depth of 6mm. A mercury thermometer was placed in the reservoir water to monitor temperature throughout experimentation. All experiments were recorded using a Nikon Digital SLR camera with a 40 mm lens placed outside the chamber.

2.2 Measurement Devices

The temperature in the chamber was measured approximately 20 cm above the fluid reservoir using the digital thermometer in the AGPtek digital temperature controller apparatus, with an error delay of about 1 minute. The humidity in the chamber was also measured 20 cm above the fluid reservoir using the digital hygrometer in the AGPtek digital humidity controller apparatus, with a measuring error of 3%. The fluid reservoir temperature was measured using a mercury-in-glass thermometer submerged in the fluid with an error of 0.5^{o}C.

2.3 Experimental Procedure

2.3.1 Paper Device Fabrication

Paper devices were fabricated from two grades (1 CHR and 17 CHR) of pure cellulose chromatography paper sheets, 20 cm by 20 cm in size. Chromatography paper was chosen due to its intended use as a lateral flow platform for analytical chemistry. The 1 CHR and 17 CHR grades were selected based on availability, thickness and the specified linear flowrate, where 1 CHR is considered the standard chromatography paper with a moderate flowrate. 17 CHR paper is the

thickest chromatography paper available, has the quickest flowrate, and is specified for chromatography applications with larger molecules, therefore, it was selected to provide contrast. Properties of 1 CHR and 17 CHR chromatography paper are given in Table 1. The porosity values are calculated using Equation 4 along with the basis weight of the paper as provided by the manufacturer, which describes the paper density per area. This equation assumes the weight of the air in the pores is negligible relative to the weight of the paper fibres. In this equation, ρ_{BW} is the basis weight of the paper, h is the thickness of the paper, and ρ_c is the density of cellulose which is typically 1.5 g/cm^3.

Table 1. Properties of Whatman chromatography paper

Paper Type	Basis Weight (g/m^2)	Thickness (mm)	Porosity	Flow Rate (mm/min)
Whatman 1 CHR	87	0.18	67.8%	4.33
Whatman 17 CHR	325	0.70	69.1%	6.33

$$\phi = 1 - \frac{\rho_{BW} h}{\rho_c} \tag{4}$$

Device dimensions were designed electronically and printed to scale onto the 1 CHR chromatography paper using an HP Deskjet 2540 inkjet printer. The 17 CHR paper device dimensions were drawn onto the paper using a graphite pencil. For every strip, markings were made along the length of the device (perpendicular to the intended flow direction) in 5 mm

increments to track flow progression in the paper during experimentation. Paper devices of both grades were cut using a guillotine paper cutter, the resulting paper device is shown in Figure 3.

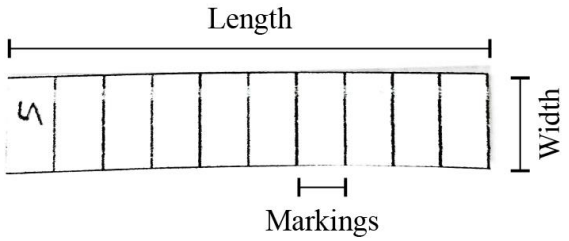

Figure 3. Paper device dimensions with 5 mm increment markings to track flow progression.

2.3.2 Reservoir Solution Preparation

To improve visibility of fluid motion in the paper strip, the water used in experiments was dyed with Allura red food colour dye at a concentration of 12.5 mmol. A low concentration was used to avoid alteration in the chemical properties of water. Stock solutions were prepared in 250 mL batches prior to experiments, stored at room temperature, and replenished as necessary. Allura red was purchased in powdered form from Sigma-Aldrich, and has a molar mass of 496.42 g/mol. To obtain a concentration of 12.5 mmol in a volume of 250 mL, 1.55 g of Allura red is required. Using a digital balance scale, 1.55 g of Allura red powder was measured and placed in a 250 mL volumetric flask. Distilled water was added to the volumetric flask in increments, and thoroughly mixed with each increment to ensure complete dissolution of the dye in the water and an even distribution of dye particles throughout the solution.

2.3.3 Introduction of paper sample to fluid reservoir

A Nikkon Digital SLR was mounted on a tripod outside the chamber. To prepare the fluid reservoir, a petri dish was placed in the chamber and filled with the dyed water. The dyed water was replaced after each set of experiments for consistency. The temperature and humidity conditions of the chamber were set, the chamber was sealed and allowed to reach steady state. Meanwhile, the camera angle and focus were adjusted. Experiment recordings began once the temperature and humidity conditions in the chamber were steady. A paper sample was folded at the first 5 mm marking, the 5 mm below the fold was submerged in the fluid reservoir as shown in Figure 4. Any fluctuations in chamber conditions during experiments were noted. Video recordings of the experiments were used to obtain measurements of the time (in seconds) at which the fluid reached each 5 mm marking along the paper strip sample. A time of 0 seconds and a distance of 0 mm was assigned where the fluid passed the fold in the paper sample.

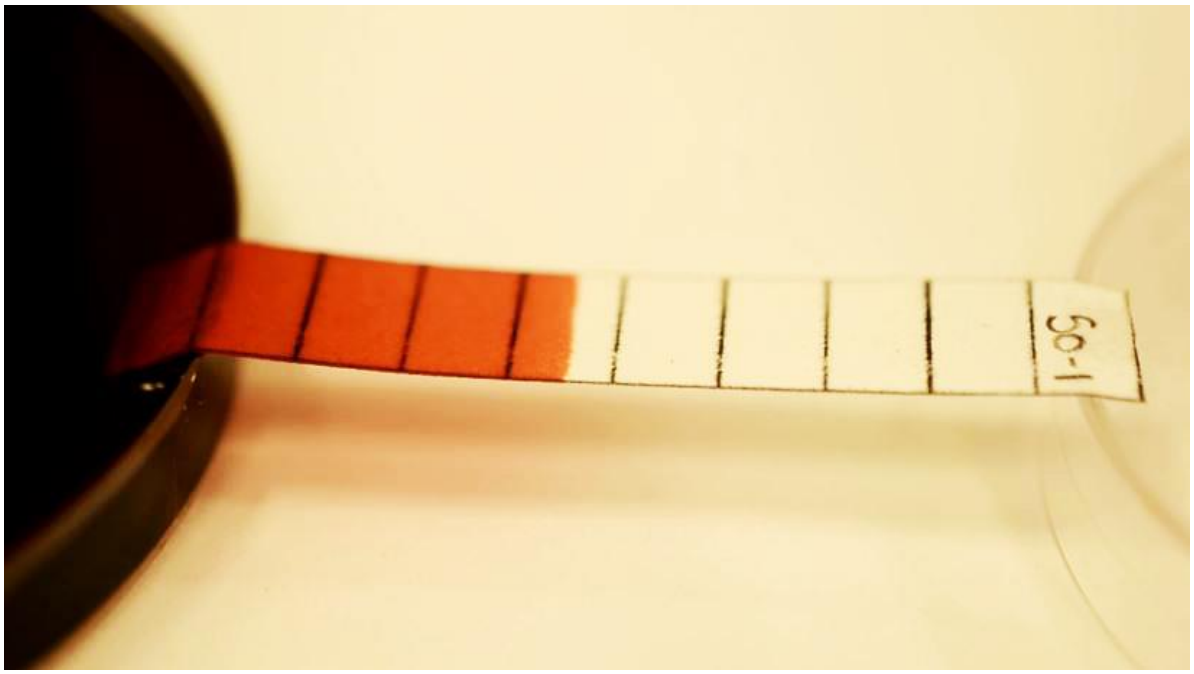

Figure 4. Photograph of 1 CHR paper strip in contact with the fluid reservoir during experiment to observe wicking behaviour

2.3.4 Sample Size

Each data set contained four samples for statistical significance. During preliminary experimentation, sample sizes of four, six, and ten were tested, demonstrating similar values for standard deviation and error. Thus, a sample size of four was selected to optimize the time efficiency of the experiments. A standard error was calculated for experimental data, and is represented by error bars in all graphical representations of the experimental data in this study.

2.3.5 SEM Imaging

To obtain a visual depiction on the microscale of the fibrous medium being investigated, a JEOL 6400 scanning electron microscope (SEM) was used to take micrograph images of Whatman 1 CHR and 17 CHR chromatography paper, as well as Whatman 1 filter paper since it is commonly referred to in relevant literature. A 5 mm square piece was cut from each type of paper and placed on an aluminum stub 9.5 mm in diameter and 9.5 mm in height, using double sided carbon tape to eliminate interference from the aluminum stub. Each sample was sputter coated with an ultra-thin layer of gold to prevent charging of the paper samples during imaging.

Chapter 3

Results and Discussion

In this chapter, experimental results for parameters that impact fluid behaviour during wicking are presented and discussed. The parameters investigated include ambient conditions using temperature and humidity, and paper geometry in terms of length, width, and machine direction.

3.1 SEM Imaging

Mathematical models for fluid flow in paper are based on the Washburn equation or Darcy's law, which both contain a term reflecting the pore size of the paper. To gain a physical understanding of pore and fibre structure of paper, and how it may influence flow, a scanning electron microscope (SEM) was used to obtain micrographs of paper. Of particular interest was the pore and fibre geometry that some models have incorporated into their mathematical description of flow behaviour.

Three different types of paper were imaged as shown in Figure 5, the Whatman chromatography 1 CHR and 17 CHR grades used in experimentation for this study, and the Whatman 1 filter paper as it is commonly used in μPAD designs. The micrographs were taken at 2 to 4 different magnifications to observe the details of the microscale paper fibre structure. For

the 1 CHR paper in Figure 5a, two micrographs at the 20 μm scale are included to portray the variety of pore shapes and sizes that can be seen in two different locations on the same piece of paper. For the same reason, the 17 CHR paper in Figure 5b shows micrographs at 20 μm and 10 μm where differences in pore and fibre appearance at two different locations on the paper are evident. A key observation from each of the SEM micrographs is that the micro-structure of paper cannot accurately be represented by the bundle of cylindrical capillaries approximation, especially considering the practical challenge of selecting an appropriate representation of capillary radius. It can also be observed that in each of the three types of papers, pore sizes range from 0.1 μm to 50 μm. Though there are differences in the paper properties provided by the manufacturers, as shown in Table 1, it is difficult to correlate these properties to the SEM micrograph visuals. According to the manufacturer, the 1 CHR paper and filter paper have the same porosity, whereas the 17 CHR has a slightly lower porosity [54], [55]. However, it is unclear how to assign a porosity value to the fibre network structure observed in the SEM micrographs. A closer look at the micrographs shows some interesting differences in the structure of the fibres themselves. At the nanoscale, it can be seen that the large paper fibres are made up of smaller fibres intertwined, and fibres as small as 10 nm in diameter were detected. This observation in fibre structure reiterates the complexity of the fibre network structure of paper, and emphasizes the complication involved in assigning a representative average pore size. It also calls to question the extent to which fibre dynamics could influence the fluid motion through the paper network, and is a concept of interest recommended for further investigation.

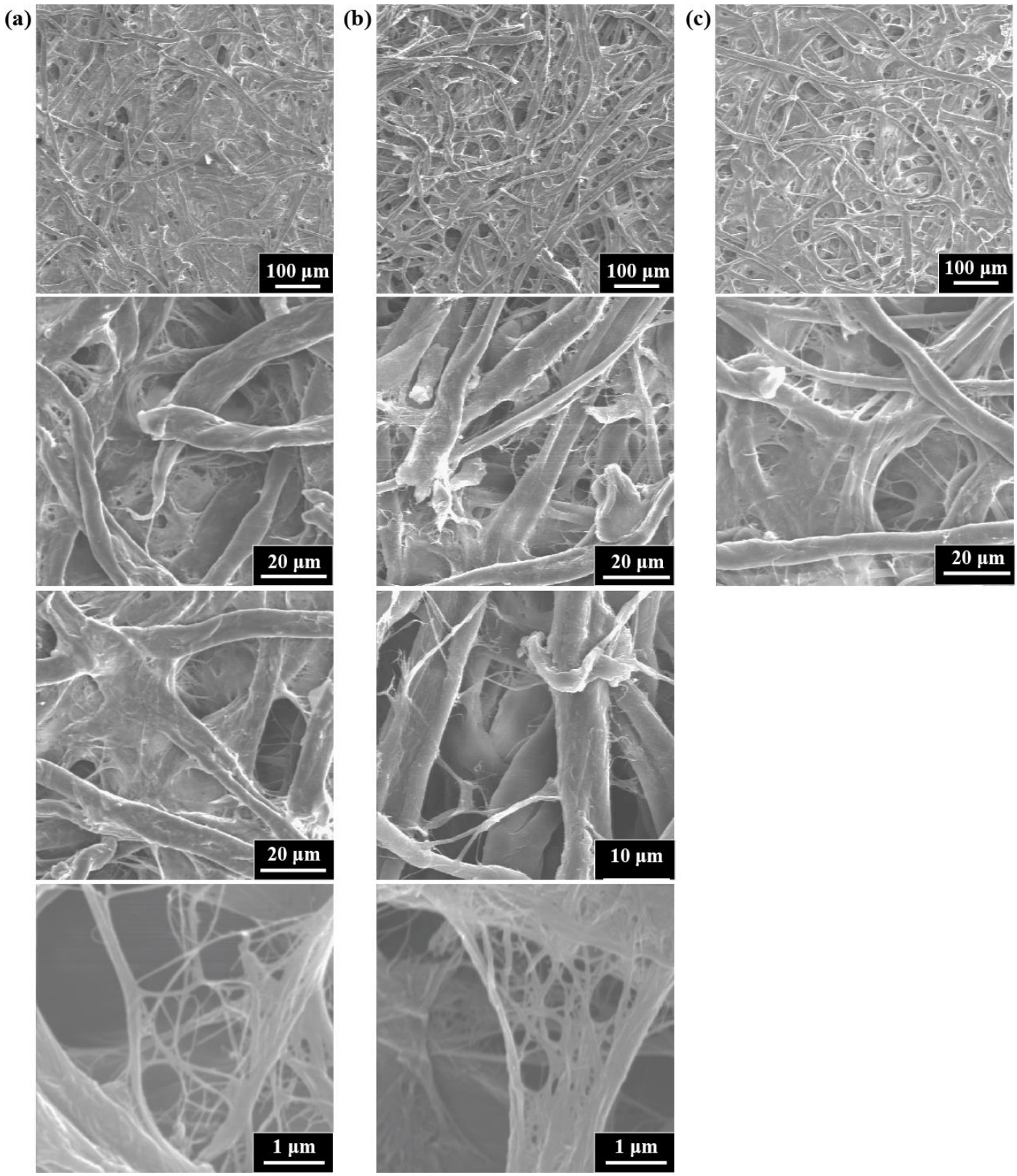

Figure 5. SEM micrographs of (a) Whatman 1 CHR chromatography paper, (b) Whatman 17 CHR chromatography paper, and (c) Whatman 1 filter paper.

3.2 Machine Direction

When chromatography papers are purchased, a machine direction is indicated on the paper by the manufacturer. Machine direction is determined by the direction in which the paper pulp fibers are laid into sheets during the production process. Since the paper fibre structure is complex and difficult to characterize, it is possible that this property specified by the manufacturer may provide insight on the fibre structure, and is therefore examined to determine its impact of fluid flow behaviour.

In studies that investigated paper production, it was observed that the paper fibers had a tendency to align parallel to the machine direction [23], [56]. To confirm this observation, the SEM micrographs can provide insight on fibre arrangement relative to machine direction. Figure 6 indicates the machine direction in both the 1 CHR and 17 CHR chromatography papers. The filter paper was purchased in circular sheets and a machine direction is not typically indicated or necessary in filtering applications. While there exists fibres in all directions of the paper, a general trend in alignment direction can be observed in the micrographs for the chromatography papers that correspond to the machine direction.

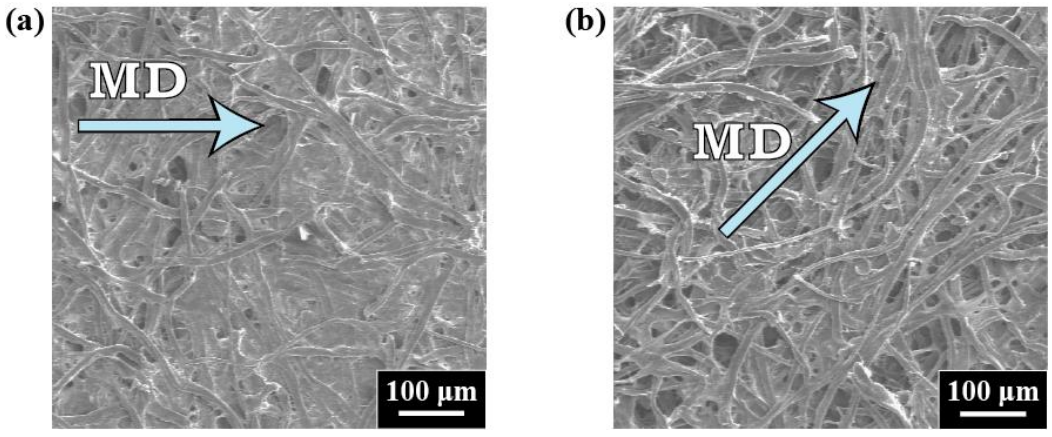

Figure 6. Machine direction indication on SEM micrographs for (a) 1 CHR and (b) 17 CHR chromatography papers

Intuitively, it is expected that fluid motion along the length of the fibres will encounter less flow resistance and therefore wick in a shorter time. This would be especially true if Roberts' observation is applicable and the dominant flow mechanism is capillary-driven flow along the channels formed by adjacent fibres [25]. Figure 7 compares the wicking time in cross-machine and machine direction 17 CHR paper strips 10 mm in width. These results demonstrate that the total wicking time for the paper strip in the cross-machine direction is approximately a 30% slower than the machine direction strip. One can hypothesize that the fibres laying perpendicular to the flow direction retard the wicking process. Considering the mechanism responsible for this decrease in wicking time is unclear, and that the chromatography paper is manufactured for intended use in the machine direction, experiments were conducted with paper strips fabricated in the machine direction.

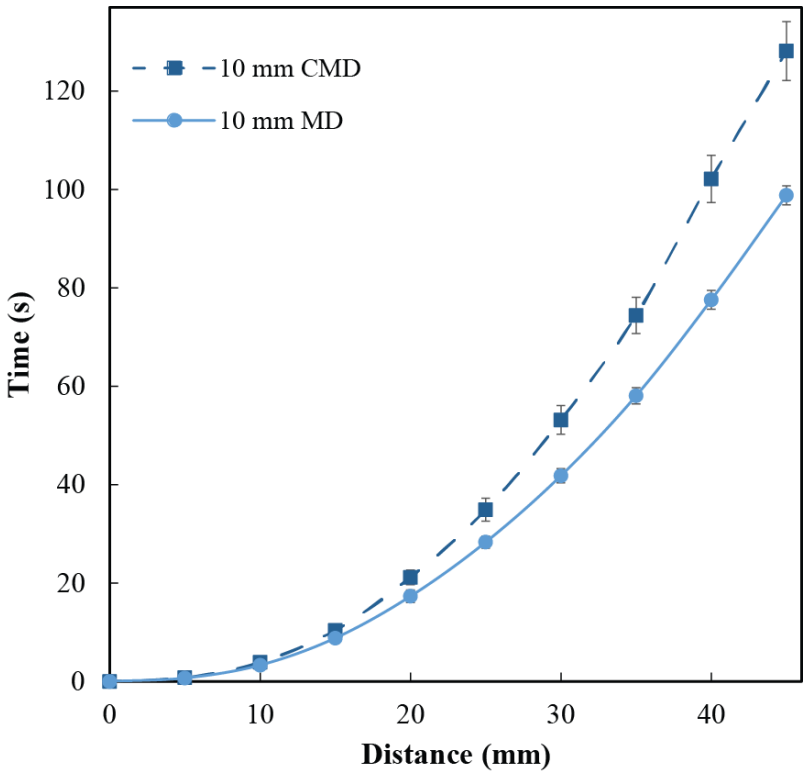

Figure 7. Comparison of experimental results for wicking in a 10 mm wide 17 CHR paper in the machine and cross-machine directions.

3.3 Temperature

The influence of temperature on fluid flow behavior in paper was investigated by observing wicking time in a paper strip 10 mm in width and 45 mm in length at a fixed humidity of 30% and temperatures varying from 15°C to 50°C to reflect the temperature range in Bangladesh. Figure 8 shows the data obtained from this set of experiments. It should be noted that the fluid reservoir temperature was typically lower than the ambient temperature in the chamber, and is shown in brackets next to the ambient temperatures. The results show a strong correlation between temperature and wicking time, where an increase in temperature corresponds to a decrease in total wicking time. Here it can be observed that the experimental data reflects Darcy's law where the wicking distance is inversely proportional to the root of viscosity, and the viscosity is a function of temperature.

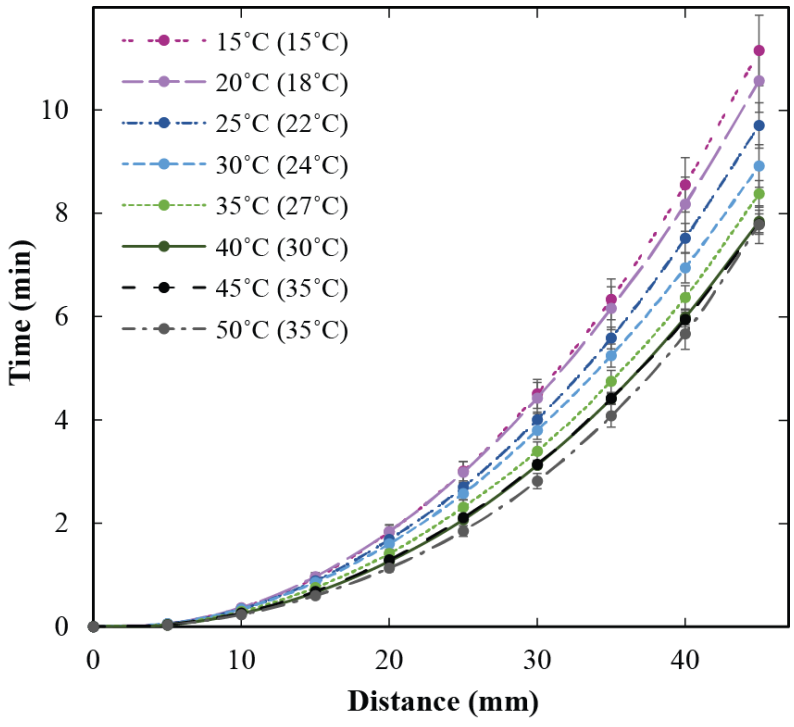

Figure 8. Experimental data for wicking in 1 CHR strips at 30% humidity and temperatures varying from 15°C to 50°C.

Since viscosity is a key parameter in Darcy's law (Equation 3), the validity of this correlation can be further explored graphically. Figure 9 compares the wicking distance at 6 minutes with the reciprocal of the square root of viscosity, as it appears in Darcy's law, at each fluid temperature in the experiment.

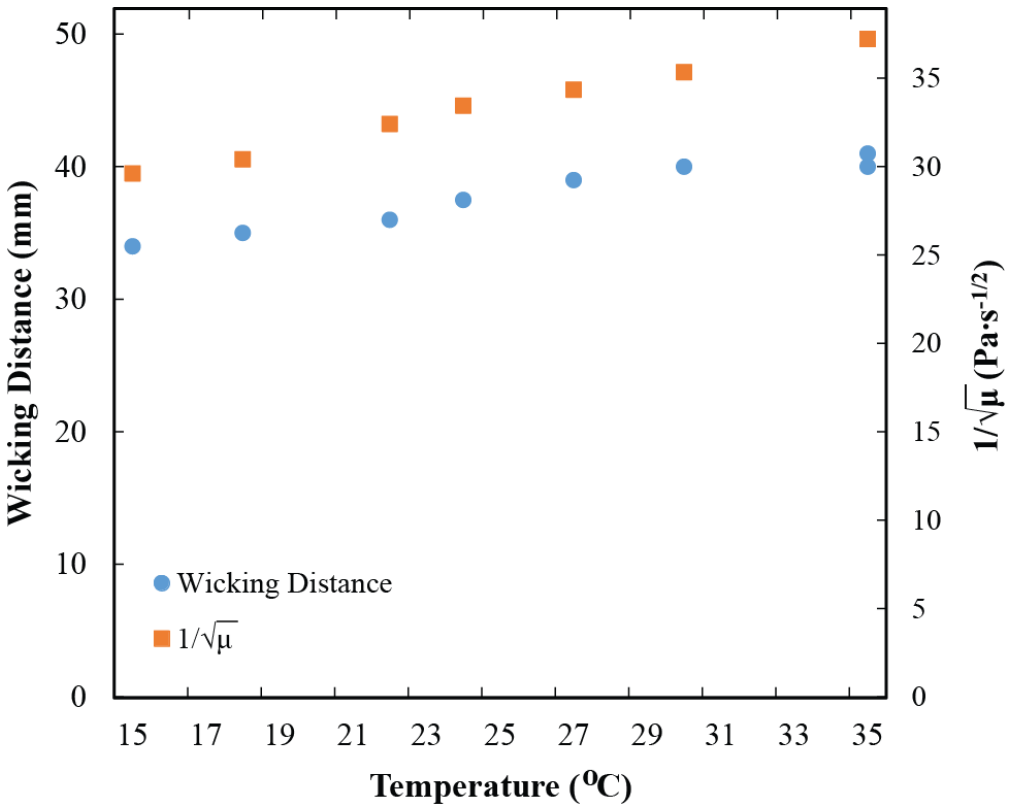

Figure 9. Comparison of wicking distance in 1 CHR paper 10 mm wide, and viscosity with temperature.

It can be concluded that the fluid viscosity, and subsequently its temperature, is a significant parameter in the flow behavior in a paper medium. It should be noted that the ambient temperature was not found to impact flow behaviour in the paper device, as the viscosity changes associated with the fluid temperature can account for the variations in wicking time observed experimentally. When designing μPADs where a controlled flow or a specific wicking time is required, it is

imperative that the temperature of the fluid being wicked, and its corresponding viscosity, are taken into consideration.

3.4 Humidity

Some μPAD designs incorporate an enclosure for the paper component of the device where evaporative effects were thought to significantly impact flow behaviour [29], [40], [57]. In fact, poor sample retention in paper microfluidic devices due to sample evaporation during transport was identified as a limitation of paper-based microfluidic technology in a recent review [58]. To gain a complete understanding of the impacts of ambient conditions, the effect of humidity on wicking in paper strips was investigated. The wicking time in paper strips 10 mm in width and 45 mm in length was investigated at a temperature of 25^{o}C and relative humidity conditions ranging from 30% to 85%. Figure 10 depicts the resulting data from these experiments. Due to the 3% reading error in the humidity controller, and fluctuations due to opening and closing of the chamber door, experiment conditions were maintained within a 5% range. In general, the paper strip had a total wicking time of approximately 7 minutes, with no distinct correlation with changes in humidity.

These results can conclude that there are no observable impacts of humidity on wicking of fluid in a paper strip. Additionally, any evaporative effects on the fluid as it flows through the paper can be deemed negligible for the conditions of these experiments. In terms of the paper-based arsenic test design, the impacts of humidity and evaporation during wicking do not need to be considered or addressed in the mathematical model for fluid flow behaviour in paper.

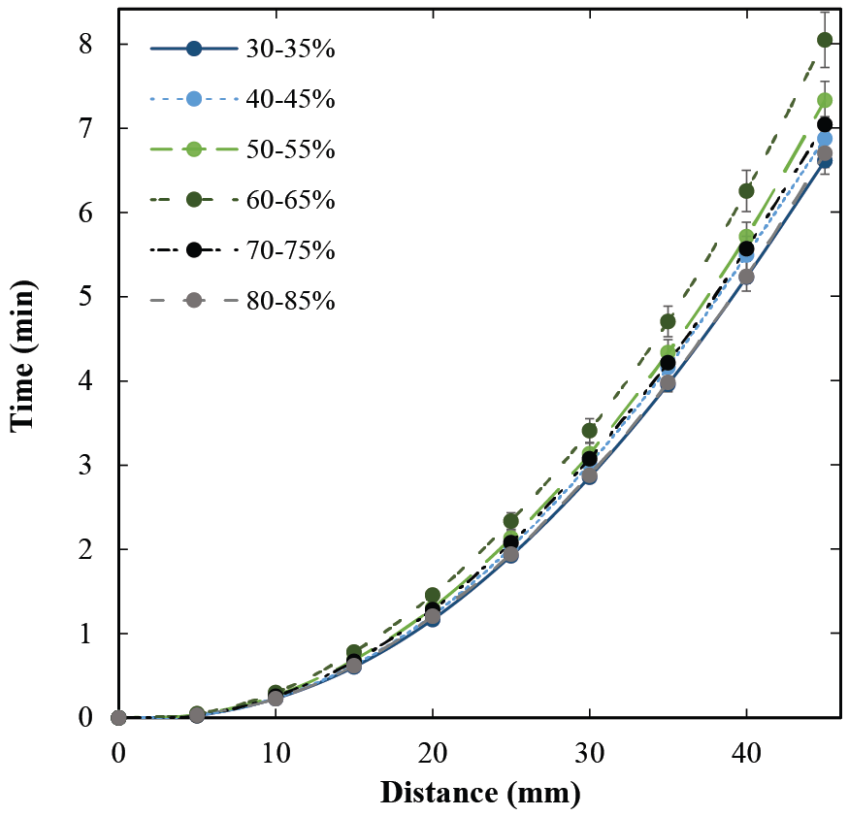

Figure 10. Experimental data for wicking in 1 CHR paper 10 mm in width at 25°C, with humidity varying from 30% to 85%.

3.5 Width

Some studies have shown that the width of a paper, has an impact on flow behaviour [48], [51], [59]. These studies demonstrated contradicting conclusions, Songok et al. found that increasing the width of the paper decreased the wicking velocity [48] while Bohm et al. observed an increase in wicking velocity with increasing width [59]. Additionally, both the Washburn equation and Darcy's law do not include a width parameter. Further investigation of the influence of width on fluid flow behaviour in paper is necessary, such that it can be appropriately incorporated into the mathematical model to be developed.

To study the influence of width of the paper strip on fluid flow behaviour, wicking time was observed in 1 CHR paper strips 0.18 mm in thickness, 45 mm in length and a range of widths from 5 mm to 40 mm. In order to expand the range of cross-sections in the experiments, wicking was also observed in 17 CHR paper strips 0.7 mm in thickness, 45 mm in length, and a range of widths from 5 mm to 30 mm.

Experimental results for the 1 CHR strips are given in Figure 11. This data exhibits that there is a decrease in total wicking time as the width of the paper strip increases. At a width of 25 mm (± 2 mm) and higher, there was no longer variations in the wicking time, indicating that 25 mm (± 2 mm) is a critical width value for the 1 CHR paper strip. The ± 2 mm measurement error is a result of the thickness of the lines printed onto the chromatography paper that outline the device border, as well as the thickness of the paper cutter blade, which both cause slight variations in cutting accuracy. For a thickness of 0.18 mm, this critical width corresponds to a critical cross-sectional area of 4.5 mm^2 (± 0.36 mm^2). A concept of interest here are the length scales involved in this system. The fibre network and pore structures of the paper vary from the nanometer scale to the millimeter scale, as seen in the SEM micrographs in Figure 5, whereas the width changes are on the millimeter scale. In the presence of multiple active length scales, any physical dependencies are thought to decouple and a relationship between two dimensions on different length scales is not expected. Since the fibre network structure is complex, and its specific effects on fluid behaviour have yet to be well understood, the idea of fluid pathways can be implemented to explain these observations. As the cross-sectional area of the strip increases, more interfibre pathways are made available for the fluid to select a pathway of least resistance, subsequently facilitating permeation and allowing for a quicker wicking time. Above the critical cross-sectional area, the statistical distribution of available pathways no longer increases and no further decreases in wicking time are observed. In this sense, any variations in wicking time corresponding to

changes in width are presumably due to resulting changes in the statistical availability of favourable fluid pathways.

Figure 12 gives experimental data for the 17 CHR strips. Here the results illustrate that there are no variations within the margin of error in wicking time with changes in width. For a paper thickness of 0.7 mm, the 5 mm (± 2 mm) width strip gives the smallest corresponding cross-section value tested for the 17 CHR paper of 3.5 mm^2 (± 1.4 mm^2).

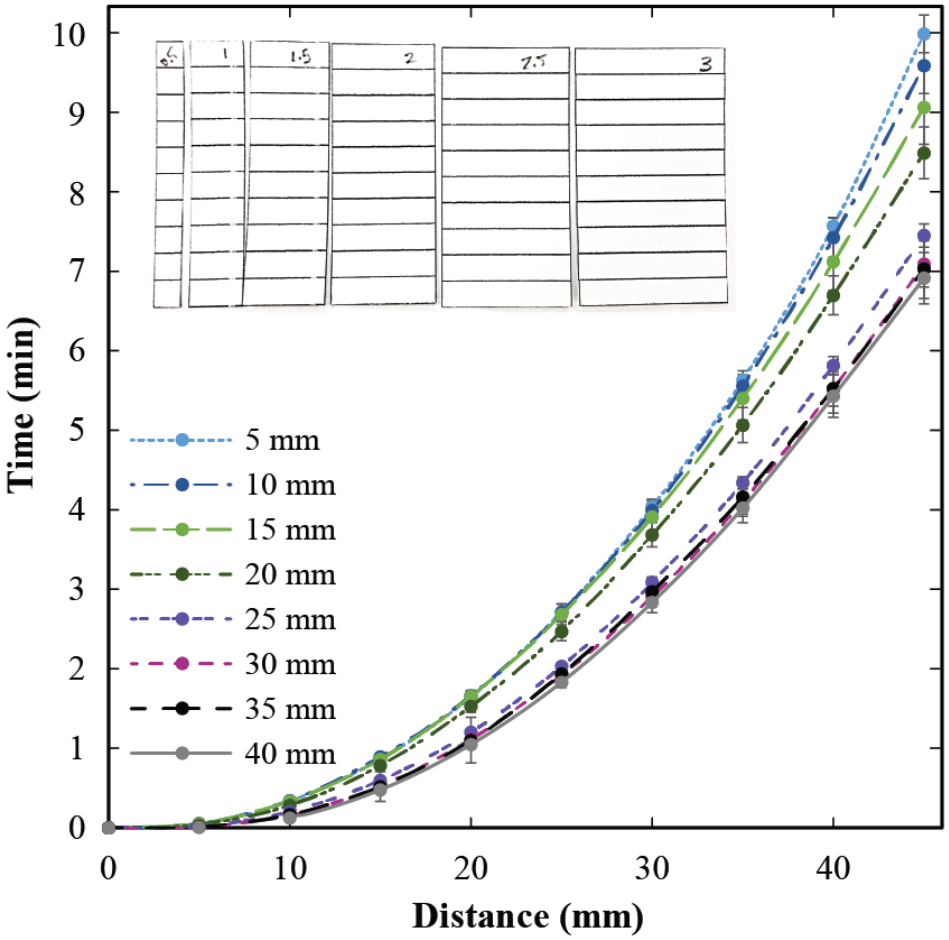

Figure 11. Experimental data for wicking in 1 CHR paper strips varying in width from 5 mm to 40 mm.

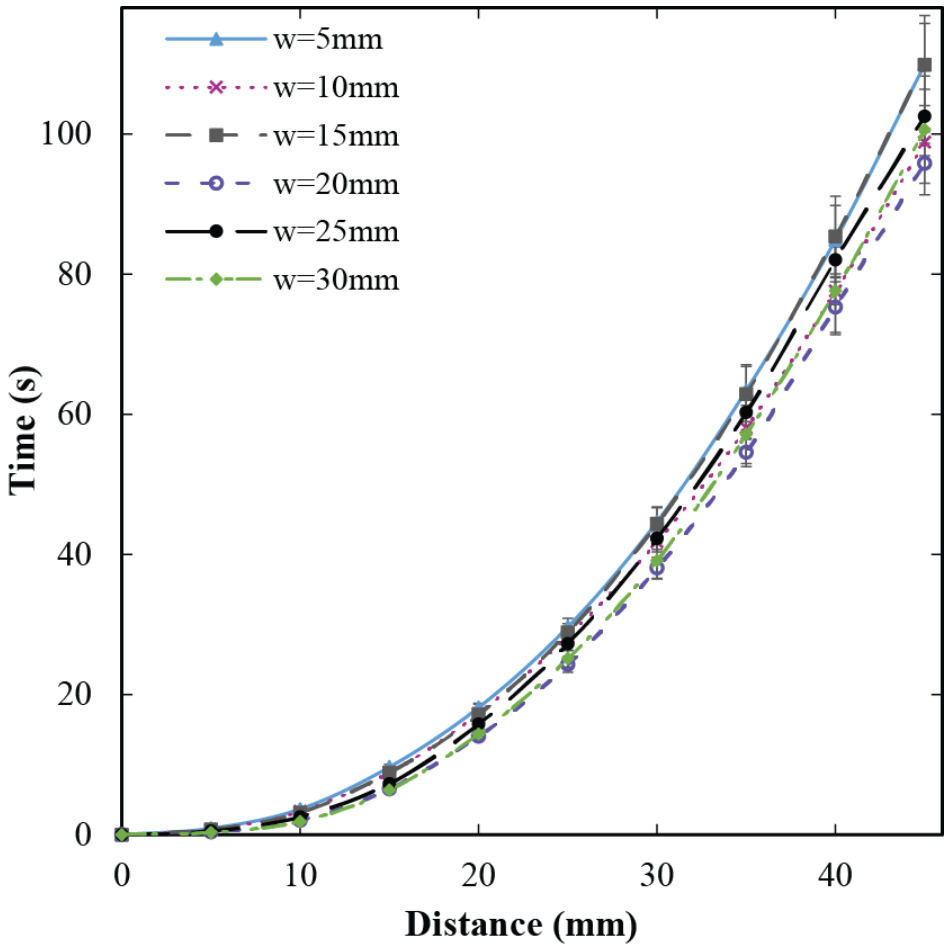

Figure 12. Experimental data for wicking in 17 CHR paper strips varying in width from 5 mm to 30 mm.

These results conclude that fluid flow behaviour in paper is sensitive to the width of the paper strip, or more generally the cross-sectional area. The wicking time decreased for increasing width in 1 CHR and 17 CHR strips below the critical cross-sectional area. The influence of cross-sectional area on fluid flow behaviour make it a key parameter that should be incorporated in the mathematical model to be developed. When designing μPADs, the critical cross-sectional area of the selected paper needs to be identified, so that device dimensions can be chosen according to the desired wicking time.

3.6 Length

Paper geometry also includes the length of the paper strip, as μPADs may need to be designed to fit a certain enclosure or size constraint. Experiments to inspect the influence of the length of the strip were conducted using 1 CHR paper strips 10 mm in width and lengths varying from 25 mm to 65 mm.

Results are graphically represented in Figure 13, which demonstrate similar flow behaviour for paper strips of different lengths. This indicates that any additional length of paper does not influence the driving pressure gradient or the resistances to flow. This is because the pore network

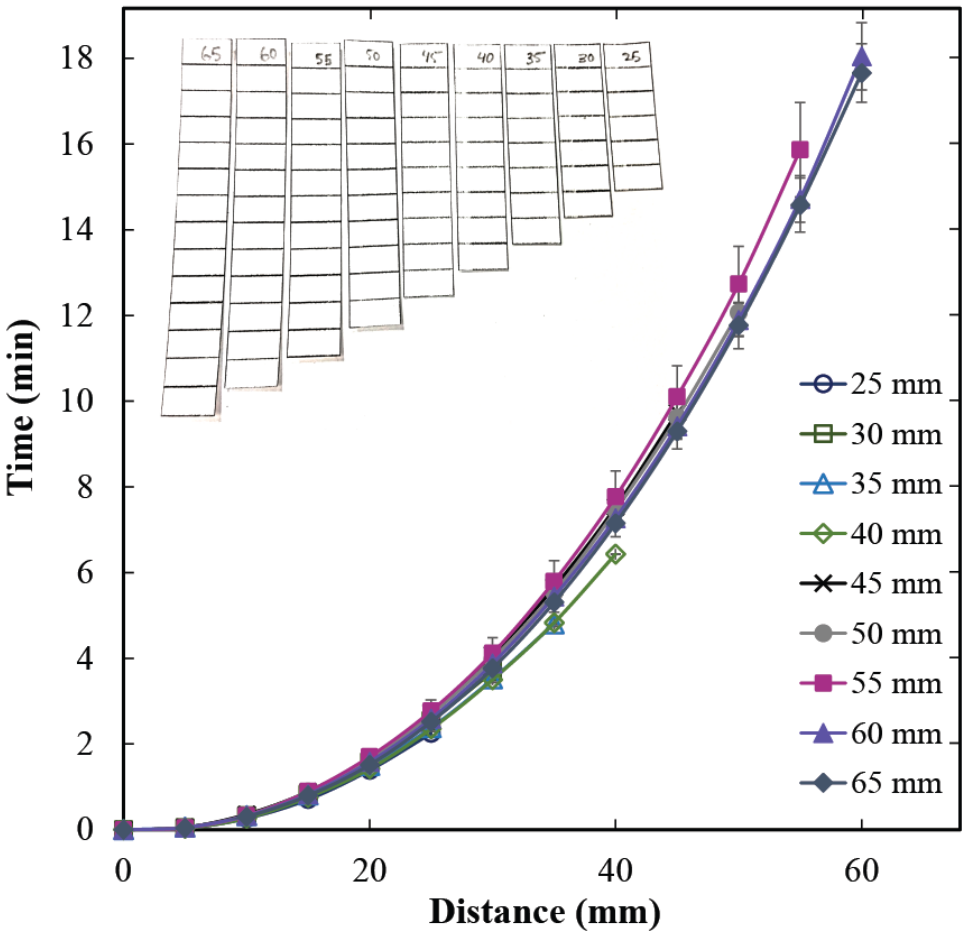

Figure 13. Experimental data for wicking in 1 CHR paper strips 10 mm in width and length from 25 mm to 65 mm.

in the paper is open to the atmosphere, such that the air displaced by the imbibing fluid can leave the paper strip rather than accumulating within the pore network and affecting the flow mechanism.

In summary, these results conclude that the length of a paper strip does not impact flow behaviour and is, in consequence, a flexible parameter when designing μPAD. In developing a mathematical model to predict flow behaviour in paper, a length parameter should not be incorporated. When designing a μPAD, the length dimension of the device can be adjusted to accommodate any spatial requirements without changing the flow behaviour in the device.

3.7 Post-Wetting Flow

Post-wetting flow was first observed in a paper strip that was left in contact with the reservoir several minutes after an experiment run had been conducted to observe wicking behaviour. The paper-strip had darkened in colour, possibly indicating the presence of an increased volume of dyed water. A change in the volume of water within the paper device that is not accounted for would result in false test results, therefore, the occurrence of post-wetting flow was further investigated.

After the fluid had wicked the full length of the strip, paper devices remained in contact with the reservoir while the camera continued its recording, in an effort to observe post-wetting flow. Though no additional fluid wicking was expected, there occurred a visually detectable increase in the dye content of the paper strip, or a darkening in colour. Experiment videos were analyzed using ImageJ to verify and quantify the colour change in a 1 CHR paper strip. Once the fluid front had travelled to the end of the strip, snapshots of the video were taken in 1 minute increments for a duration of 17 minutes while the strip remained in the reservoir.

Snapshots from the 0 minute and 17 minute marks, as shown in Figure 14, were analyzed in ImageJ using the Histogram function to obtain a colour profile of the red tone of the paper strip. With this function, the intensity of the red colour is measured by detecting the redness of each pixel and assigning it a value from 0 to 255, where 0 is the darkest pixel and 255 is the brightest red pixel. The number of pixels at each value is then plotted to give the colour profiles shown in Figure 15. A comparison of these red colour profiles at 0 and 17 minutes shows a substantial shift in the profile to the left, reflecting the visually detected darkening in colour.

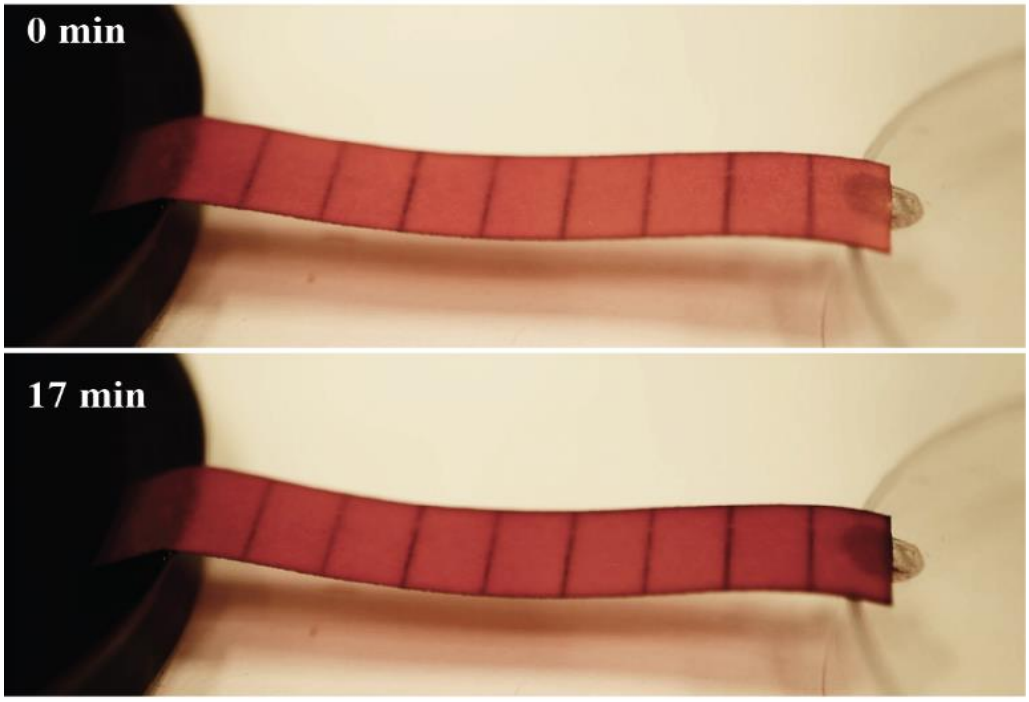

Figure 14. Snapshots at 0 and 17 minutes after wetting in a 1 CHR paper strip that remains in contact with the reservoir.

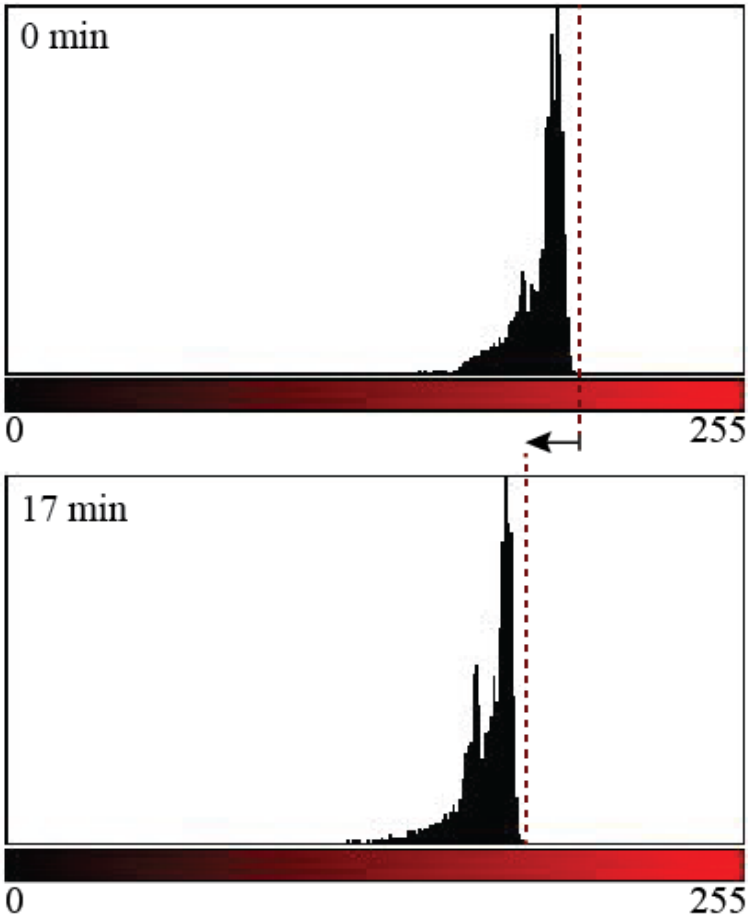

Figure 15. Red tone colour profile comparison in 1 CHR paper strips at 0 minutes and 17 minutes after wetting.

The snapshots at every minute were analyzed using the same Histogram function, and the maximum value for pixel colour intensity (the value of the rightmost point on the colour profile) was recorded to quantify this observation. Figure 16 shows the results of this analysis, where the data reveals an exponentially decreasing relationship between time and brightness that approaches a minimum value for the red colour in the paper strip. This minimum value indicates that there is a maximum quantity of water that can be retained by the paper device during post-wetting flow.

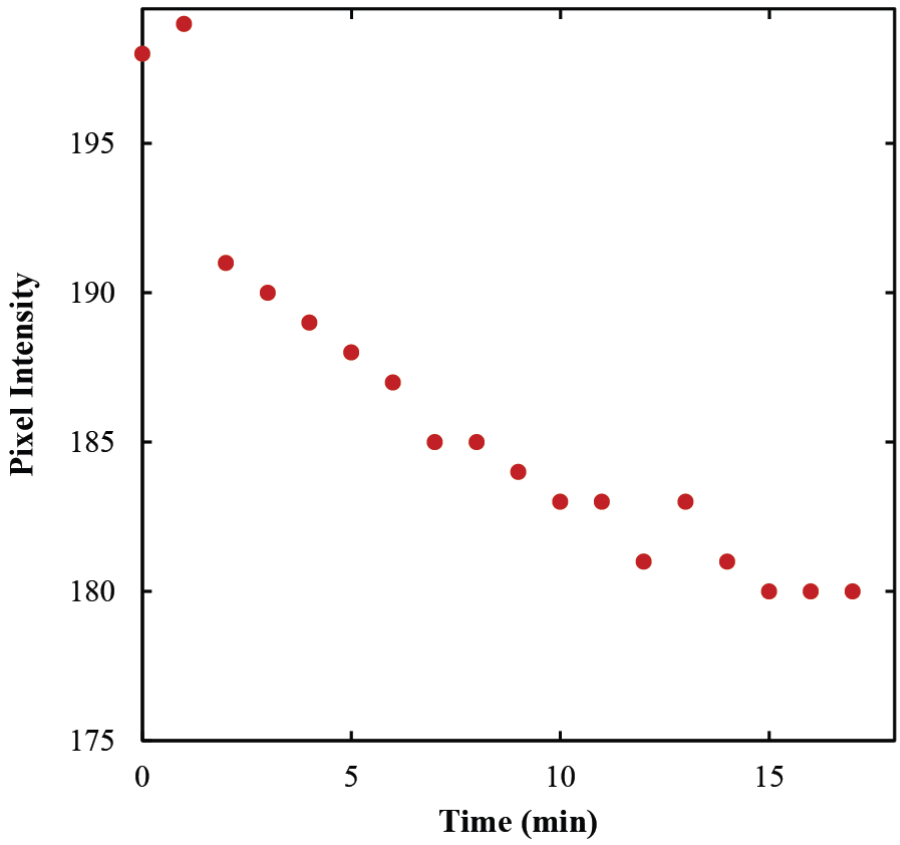

Figure 16. Changes in red pixel intensity over time after wetting in 1 CHR paper.

To ensure this observation can be considered post-wetting flow rather than a diffusion of dye molecules, results were compared to a paper strip that was removed from the reservoir and recorded for the same duration of time. The strip at 0 and 17 minutes after wetting are shown in Figure 17, with the corresponding red colour profiles in Figure 18, and a plot of the maximum value for the red colour in the paper strip over time in Figure 19. A visual analysis of the strips at 0 and 17 minutes shows a very slight change in the red colour of the paper, which can be interpreted as a redistribution of dye particles within the strip. The colour profiles at 0 and 17 minutes confirm this interpretation. In these colour profiles the maximum value remains consistent while the pixel

intensity distribution changes, as demonstrated in the profile at 17 minutes by the multiple increases in height for pixel intensity values less than the maximum value. Additionally, the mass of both paper strips were measured 17 minutes after wetting, and the paper strip that experienced post-wetting flow from reservoir was 36% higher in mass than the paper strip that was removed from the reservoir.

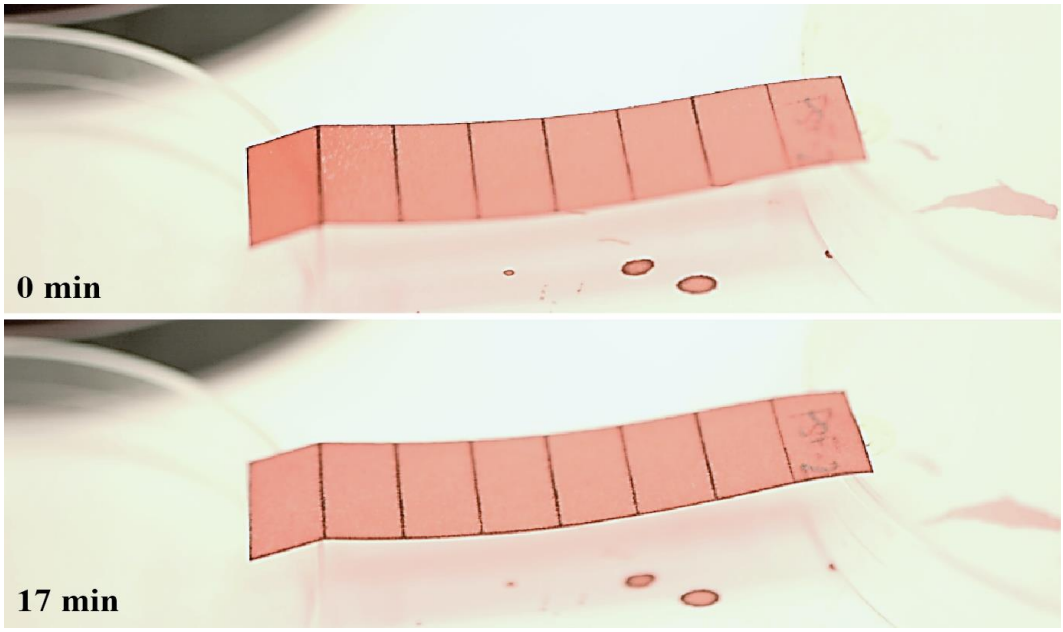

Figure 17. Snapshots at 0 and 17 minutes after wetting in a 1 CHR paper strip removed from the reservoir.

The post-wetting flow mechanism can be hypothesized by taking a close look at the SEM micrographs in Figure 5. As previously observed, the paper fibers are made up of smaller fibers intertwined. The pores in the paper are created by spaces in between the large fibers, but there are also smaller pores created by the spaces between the smaller fibers, which is responsible for the large variation in pore sizes. It is possible that the fluid wicks primarily along the fibre channels,

filling the larger interfibre pores first. During post-wetting flow, fluid moves into the intrafibre pores and the remaining void volume is filled. In the cases where the paper strip is removed from the reservoir, stretching or relaxation of the flexible paper fibres can cause fluid to redistribute within the paper strip.

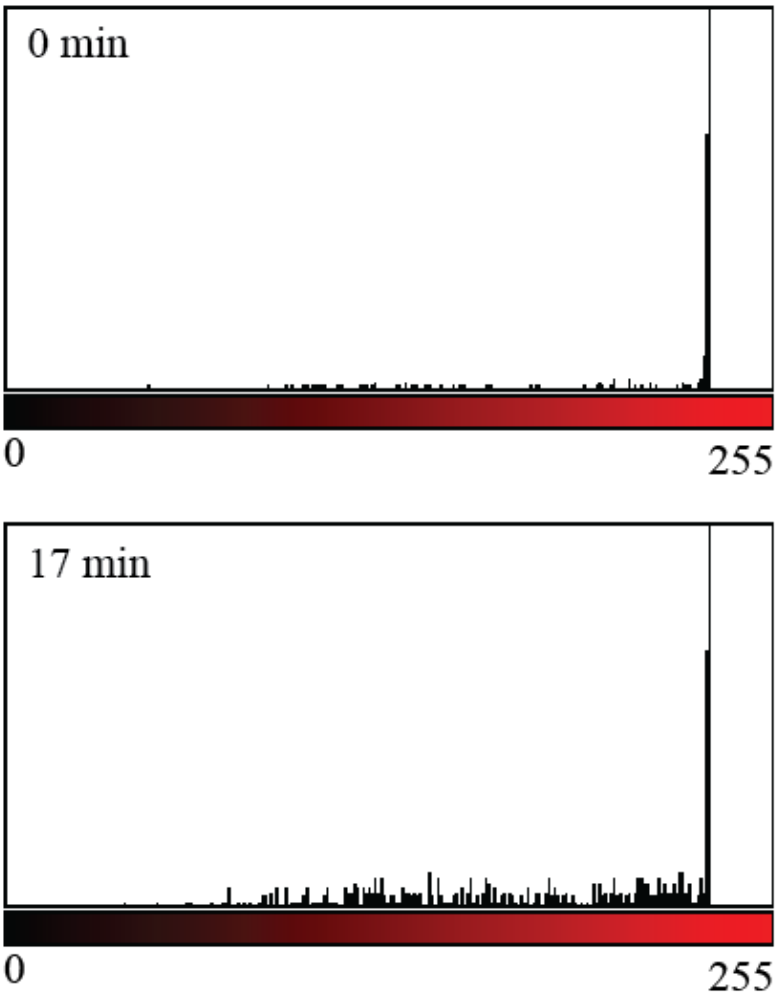

Figure 18. Red tone colour profile comparison in 1 CHR paper strips at 0 minutes and 17 minutes after removal from reservoir upon full wetting.

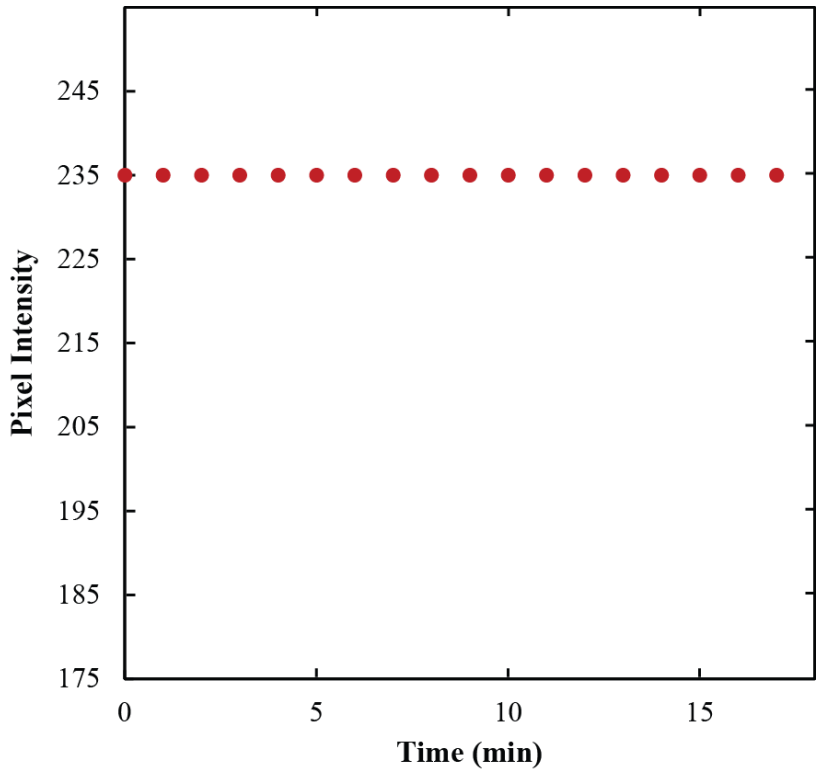

Figure 19. Changes in red pixel intensity over time in 1 CHR paper removed from the reservoir after wetting.

In the context of paper-based microfluidic device design, post-wetting flow will influence the concentration of constituents in the paper device and the intensity of the resulting signal readout. The submersion time, as well as the elapsed time prior to test readout are important considerations in paper-based microfluidic device design to select the correct quantity of reagents for a highly sensitive and selective detection reaction. Another crucial concern in the design of a paper-based microfluidic device is communicating to the user the ideal submersion time and signal readout time for the test to provide the most accurate results.

Chapter 4

Fluid Flow Model

A mathematical model that can accurately predict flow behaviour in paper-based microfluidic devices is an essential tool in the device design process. An effective model can be used to determine the optimal location and quantity of the reagents on the paper strip. The correct placement and proportions of reagents will result in a sensitive, selective, and reliable paper-based microfluidic device. In this chapter, a mathematical model is developed based on experimental findings.

4.1 Washburn Equation

The Washburn equation is applied when describing capillary-driven flows, which is the type of flow that occurs in paper. Previous studies have explored adaptions of the Washburn equation to capillary-driven flow in paper. This section reviews the fundamentals of the Washburn equation and its adaption for porous media to develop an understanding of implications associated with applying the equation to flow in paper.

4.1.1 Assumptions

The following assumptions are applied in the derivation of the Washburn equation.

- Flow in capillaries is continuous, fully developed, steady, and laminar throughout the length of the capillary.
- The capillaries are cylindrical and of constant radius.
- The liquid in the capillary is incompressible, with a constant viscosity and contact angle.
- There is no slip at the walls of the capillary, and the fluid has a finite velocity at the center of the circular pipe.
- The driving pressure gradient is linear in the x-direction, and constant with respect to time.
- The effects of gravity are negligible
- The effects of hydrostatic and atmospheric pressures negligible relative to capillary pressure

4.1.2 Derivation

This section summarizes the derivation method implemented by Washburn as depicted in his 1921 Physical Review publication. The system being modelled is described as a tube with one end in contact with a liquid reservoir and the other end open to the atmosphere. Washburn establishes that the laminar flow conditions in small capillaries satisfy conditions for Poiseuille's law for the whole flow. Poiseuille's law under the assumptions outlined in Section 4.1.1 is shown in Equation 5, as applied by Washburn, where *dV* is the volume of liquid that flows through a cross-section

$$dV = \frac{\pi \sum P}{8\mu x}(r_c{}^4 + 4\epsilon r_c{}^3)dt \tag{5}$$

of the capillary at time *dt*, *x* is the length of the column of liquid in the capillary, μ is the viscosity of the liquid, ϵ is a slip coefficient, and ΣP is the total pressure driving the liquid along the capillary. The volume term is expressed in terms of capillary radius as the volume of a cylinder as shown in Equation 6, and the total pressure is composed of atmospheric, hydrostatic, and the Young-Laplace expression (Equation 7) for capillary pressure, to give Equation 8.

$$dV = \pi {r_c}^2 dx \tag{6}$$

$$P_c = \frac{2\gamma \cos\theta}{r_c} \tag{7}$$

$$\frac{dx}{dt} = \frac{\left[P_A + \rho g h_l + \frac{2\gamma \cos\theta}{r_c}\right]({r_c}^2 + 4\epsilon r_c)}{8\mu x} \tag{8}$$

Here the γ is liquid-air surface tension, θ is contact angle, and g is the gravitational acceleration. Equation 8 can then be integrated by separation of variables, given r_c, θ, and ϵ are constant values, resulting in Equation 9. If the no slip condition applies then then ϵ is equal to zero. Washburn also

$$x^2 = \frac{\left[P_A + \rho g h_l + \frac{2\gamma \cos\theta}{r_c}\right]({r_c}^2 + 4\epsilon r_c)t}{4\mu} \tag{9}$$

states that for flow in capillaries, the atmospheric and hydrostatic pressures are negligible compared to the capillary pressure. This gives the Washburn equation in Equation 2, shown below for convenience, which is applicable to horizontal and vertical capillaries.

$$x^2 = \frac{\gamma \cos\theta}{2\mu} r_c t \tag{2}$$

4.1.3 Adaption for Porous Media

Washburn also discusses an approach to adapt the capillary flow equation for the rate of penetration of a liquid through porous body. He suggests the porous body be taken equivalent to *n* capillary tubes so that the total volume which penetrates the porous body is given by Equation 10, where P_E

$$V = \pi \sum {r_c}^2 x = \frac{\pi}{2} \sqrt{\frac{t}{\mu}} \sum \left(\sqrt{P_E + \frac{2\gamma}{r_c}} \right) {r_c}^3 \tag{10}$$

is the external pressure driving the liquid. This expression is further simplified for capillaries small enough that the capillary forces dominate and P_E becomes negligible, shown in Equation 11. Here, κ' is referred to as the degree of penetration and specified to be independent of the nature of the liquid, similar to the concept of permeability.

$$v = \kappa' \sqrt{\frac{\gamma t}{\mu}} \tag{11}$$

4.2 Darcy's Law

Darcy's law is used to describe pressure-driven flow through porous media. Paper on the microscale is made up of a network of fibres, and can be considered a porous material in the sense that void spaces, or pores, are created between the fibres. In this section, the implications of applying Darcy's law are reviewed, and the model is adapted for capillary-driven flow.

4.2.1 Assumptions

The following assumptions are made when Darcy's law is applied.

- Flow through the porous medium is continuous, steady, and laminar throughout the medium
- Fluid velocity is linearly proportional to the pressure gradient
- The fluid is incompressible, with a constant viscosity and contact angle
- The driving pressure gradient is linear in the x-direction, and constant with respect to time.
- The effects of hydrostatic and atmospheric pressures negligible relative to capillary pressure

4.2.2 Derivation

Darcy's law was derived empirically by Henry Darcy in 1856 to describe flow through sand filters and has since been applied to a variety of porous media. It states that the velocity of a fluid through a porous medium is linearly proportional to the pressure gradient across the medium by the ratio between permeability and viscosity. A theoretical derivation of Darcy's law from the Navier-Stokes equation was explored by Stephen Whitaker in 1986 [50]. Equation 3 is shown below for convenience. To apply this law to capillary-driven flow in paper, the Young-Laplace equation

$$v = -\frac{\kappa}{\mu}\nabla P \tag{3}$$

(Equation 1) can be applied as the pressure gradient. This assumes that the pressure gradient is linear in x and constant with time, and that all other pressure forces are negligible relative to capillary pressure. By separating variables and integrating, Darcy's law can be expressed in the form given by Equation 12, which is similar in form to the Washburn equation in Equation 2. A comparison of the Washburn (Equation 2) and Darcy (Equation 3) models yields the expression in Equation 13 relating permeability to capillary radius.

$$x = \sqrt{\frac{4\gamma\kappa\cos\theta}{\mu\, r_c}\, t} \tag{12}$$

$$\kappa = \frac{{r_c}^2}{8} \tag{13}$$

4.3 Model Development

To develop a mathematical model capable of accurately predicting flow behaviour in paper-based microfluidic devices, Darcy's law is applied to leverage the flexibility offered by the permeability parameter. In this section, experimental data is analyzed to develop an expression for permeability that addresses key parameters.

4.3.1 Parameter Values

The experiments were conducted with dyed water as the wicking fluid, to represent the groundwater samples that will be tested with the paper-based microfluidic arsenic detection test. Values for the liquid parameters used in the models are those of water, as listed in **Error! Reference source not found.**. The surface tension parameter represents the tension orce at the liquid-air interface for water, and the contact angle value describes the interaction between water and cellulose. Paper properties as provided by the manufacturer are listed in Table 1.

Table 2. Water properties applied in model

Property	Units	Value
Surface Tension ($\boldsymbol{\gamma}$)	(mN/m)	73.2
Contact Angle ($\boldsymbol{\theta}$)	(°)	20
Viscosity ($\boldsymbol{\mu}$, at 22°C)	(Pa·s)	9.52×10^{-4}

4.3.2 Permeability

In Darcy's law, permeability provides a robust and versatile parameter that can attempt to address the complexities of paper fibre structure and the fluid flow through it. The success of the model ultimately lies in the appropriate selection of an expression for permeability.

To avoid the use of an ambiguous pore size term, the permeability term is grouped with the radius term to be empirically determined, as shown in Equation 14. In this expression, an effective radius term (r_{eff}) is used in place of capillary radius (r_c), since the model is not being applied in the context of a bundle of capillaries. The radius term should apply to a pore or capillary size, however, since a large variation in the pore size of a paper was observed (Figure 5), the application of a single pore radius was deemed inaccurate and an effective radius was implemented in its place. This permeability group is determined empirically by plotting experimental results as x^2 in terms of capillary pressure, time, and viscosity ($P_c t/\mu$), where the value of the slope is equal to the ratio between permeability and pore radius.

$$x = \sqrt{\frac{4\gamma \cos\theta}{\mu}\left(\frac{\kappa}{r_{eff}}\right)t} \tag{14}$$

Figure 20 shows the graphical calculation and resulting permeability group values for 1 CHR paper. This analysis shows that the permeability group value for 1 CHR varies with cross-sectional area up to the critical cross-sectional area by the relationship $3.52 \times 10^{-7} a_c^2 - 8.33 \times 10^{-7} a_c + 1.22 \times 10^{-5}$ mm, after which the permeability group remains constant at 1.70×10^{-5} as shown in Figure 21. Similarly, the graphical calculation and resulting permeabilities for 17 CHR are shown in Figures 22 and 23. The 17 CHR paper demonstrates a constant permeability group value of 7.01×10^{-5} mm. Table 3 summarizes the empirically determined permeability group values for 1 CHR and 17 CHR paper.

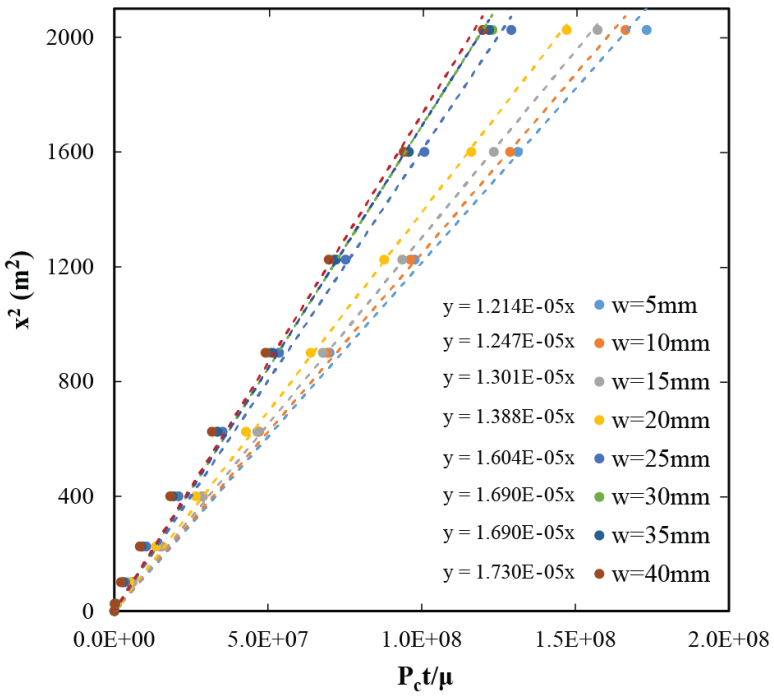

Figure 20. Graphical calculation of effective permeability for 1 CHR paper.

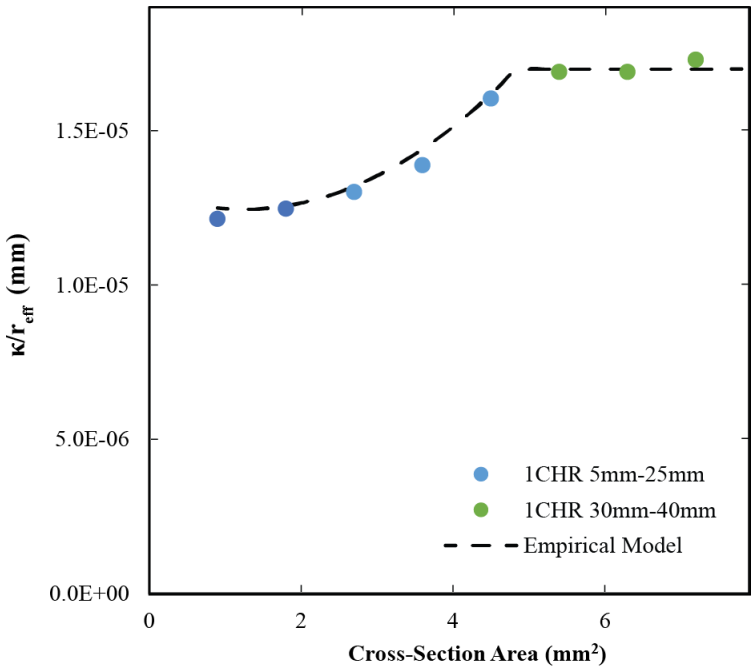

Figure 21. Comparison of effective permeability predictions with calculated values for 1 CHR paper.

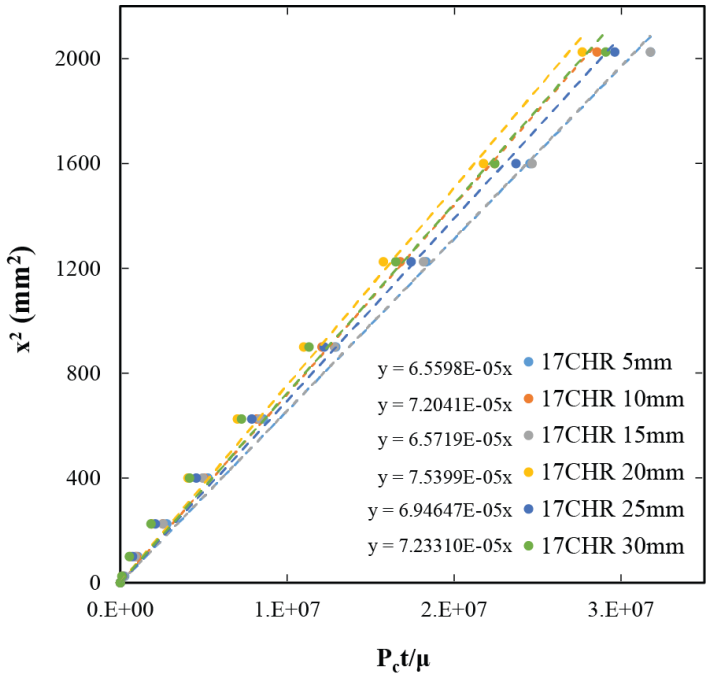

Figure 22. Graphical calculation of effective permeability for 17 CHR paper.

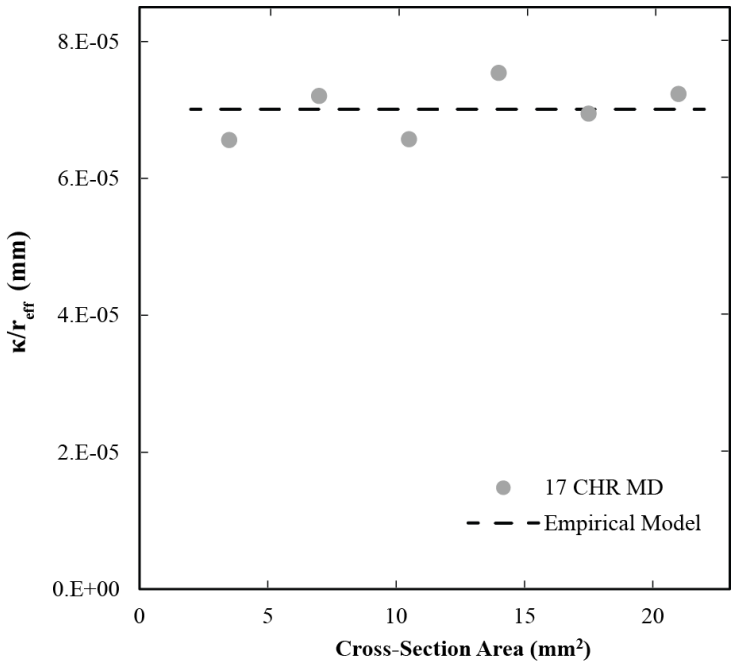

Figure 23. Comparison of effective permeability predictions with calculated values for 17 CHR paper.

Table 3. Empirical values for effective permeability in Darcy's Law

Paper Type	Cross-section Area (mm^2)	Effective Permeability (mm)
1 CHR	$a_c \leq 4.5$	$3.52x10^{-7}a_c^2 - 8.33x10^{-7}a_c + 1.30x10^{-5}$
	$a_c > 4.5$	$1.70x10^{-5}$
17 CHR	$a_c > 0$	$7.01x10^{-5}$

4.3.3 Capillary Size

Determining an appropriate representation of capillary size for a paper-based microfluidic device was an area of concern in applying the Washburn and Darcy models. In this section, experimental

results are analyzed to obtain empirical values for capillary sizes in 1 CHR and 17 CHR papers. These values are compared to approximations made in previous studies.

By applying Equation 12 and taking into consideration the empirically determined permeability group (κ/r_{eff}), the empirical values for the permeability group can be used to determine a capillary size that will reflect the experimental data for wicking behaviour in the Washburn equation. Reported pore sizes for other cellulose-based and composite papers range from 0.9 to 5 μm [28], [29], [59]. For a 1 CHR paper strip 10 mm in width, the corresponding capillary radius is 0.10 μm. Similarly the 1 CHR 40 mm wide strip has a corresponding capillary radius of 0.14 μm. In the context of this analysis, an increase in pore size is justified by the increase in permeability corresponding to increasing cross-sectional area. However, in the physical context of the paper strip, it is unlikely that the pore size increases with increases in cross-sectional area, especially since the pore size is substantially smaller than the size of the paper.

The 17 CHR 10 mm wide strip has a corresponding capillary radius of 0.56 μm. This larger pore size, relative to the 1 CHR paper, corresponds with what can be seen in the SEM micrographs. At the same time, the micrographs show a large quantity of pores that are much larger than 0.56 μm. A thorough statistical analysis of pore size distribution is required to determine an average pore size, the results can then be compared to the empirical findings in this study to determine their validity. In summary, this analysis confirms that pore size approximations required to acquire reasonable predictions from the Washburn equation are not physically intuitive.

4.3.4 Model Validation

In this section, the empirically determined expressions for permeability are applied in Darcy's law and compared to experimental data. Darcy's law with the empirical values for the

permeability group is plotted alongside experimental data for wicking in 1 CHR and 17 CHR paper in Figure 24. To confirm the validity of this model application, experimental data for wicking in 1 CHR strips 10 mm in width at 15ºC and 35ºC is shown with Darcy's law using the permeability group and viscosity values that correspond to the experiment conditions.

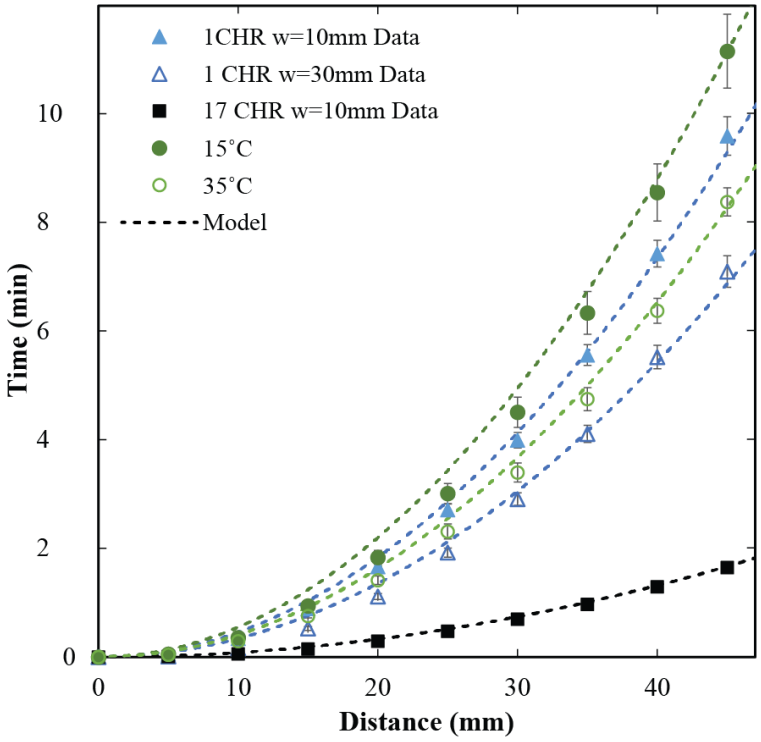

Figure 24. Application of Darcy's law using empirically determined effective permeability, and viscosity values adjusted for fluid reservoir temperature.

This model is currently limited to 1 CHR and 17 CHR chromatography paper, further experimental work should be conducted to empirically determine permeability values for any types of paper being considered as a μPAD platform. Similarly, the paper devices considered in this model are those with paper edges, or untreated edges. For devices manufactured with other fabrication methods, for example the use of wax printing or photolithography to form hydrophobic

barriers, the impacts of the barrier material and the treatments applied to the paper need to be investigated such that the model can be modified accordingly.

In summary, permeability can be used as a key parameter for predicting fluid flow in μPADs and predicting flow behaviour in paper. It is a useful metric for selecting paper types and dimensions that are appropriate for the intended application. As further research is conducted about permeability and the details of paper fiber structure, the permeability term in Darcy's law can be adjusted to address additional details.

Chapter 5

Conclusions

The findings of this thesis will be summarized in this chapter, and recommendations for future work will be put forward. The objective of this thesis was to:

- Develop a comprehensive understanding of the parameters that influence flow behaviour in a paper-based microfluidic device through experimentation, with an emphasis on the impact of ambient conditions and easy-to-modify variables such as length, width, and machine direction.

- Develop a mathematical model that accurately describes fluid flow behaviour in paper-based microfluidic devices using appropriate and measurable variables, and determine an expression for permeability that includes parameters investigated experimentally.

5.1 Conclusions

This thesis explores the performance of chromatography paper in various temperature and humidity conditions. Experiments to investigate the impacts of temperature and humidity were

conducted inside a sealed chamber with digital controllers to adjust the internal conditions of the chamber. Wicking in 1 CHR chromatography paper strips 10 mm in width and 45 mm in length was observed at temperatures ranging from 15^{o}C to 50^{o}C, with a fixed humidity of 30%. Similarly, wicking in paper strips of the same type and dimensions was observed at humidities ranging from 30% to 85%, with a fixed temperature of 25^{o}C. Experimental data concluded that changes in humidity did not affect fluid flow behaviour, therefore, the evaporative effects in the paper strip were negligible for our experiment conditions. Results from the temperature experiments demonstrated that the temperature of the fluid is an important consideration with respect to the corresponding viscosity. As the temperature of the fluid reservoir increased, the viscosity of the fluid decreased and was subsequently able to wick more quickly through the paper.

The impact of physical, easy-to-design paper parameters was also uncovered in this study. Length, width, and machine direction were varied to determine which parameters could be used to manipulate flow behaviour in a paper device. Length was varied from 25 mm to 65 mm in 1 CHR paper strips 10 mm in width, and experiment results showed now variation in wicking time with changes in length. Width was varied from 5 mm to 40 mm in 1 CHR paper strips 45 mm in length, experiments concluded that total wicking time decreased as width increased up to a critical width of 25 mm (± 2 mm) or a critical cross-sectional area of 4.5 mm^2 (± 0.36 mm^2). Strips larger than 25 mm (± 2 mm) in width exhibited no changes in wicking time. Another set of experiments was conducted with 17 CHR paper strips 45 mm in length, with widths ranging from 5 mm to 30 mm. The results show no variations in wicking speed with changes in width, indicating a critical cross-sectional area of 3.5 mm^2 (± 1.4 mm^2). In summary, cross-sectional are can be adjusted to manipulate desired wicking time, up to a critical cross-sectional area. For paper strips fabricated perpendicular to machine direction, a decrease in total wicking time was observed. Experiments were conducted with paper strips cut parallel to machine direction for consistency. In samples that

remained in the reservoir after the fluid front has wicked along the full length of the paper strip, post-wetting flow was observed. This is where the paper continues to draw fluid from the reservoir, thusly increasing the amount of dye in the paper strip. Post-wetting flow in an important consideration in paper-based microfluidic device design to ensure the correct quantities of reagents are applied and an appropriate submersion time is advised to the end user.

A mathematical model suitable for predicting flow behaviour was developed based on Darcy's law for flow in porous media. The Washburn equation for capillary driven flows may be applied to obtain an approximation of wicking time, however, the underlying bundle of capillaries assumption is fundamentally inaccurate and the capillary size approximation is not physically intuitive. Darcy's law was chosen due to the flexibility and robustness provided by the permeability parameter. Experimental data was analyzed to determine the empirical values for a permeability group in the modified Darcy's law equation, which is given by $3.52x10^{-7}a_c^2 - 8.33x10^{-7}a_c + 1.22x10^{-5}$ mm for 1 CHR strips below the critical cross-sectional area of 4.5 mm^2, $1.70x10^{-5}$ mm for 1 CHR strips above the critical cross-sectional area, and $7.01x10^{-5}$ mm for 17 CHR strips. For paper-based microfluidic device design, the use of Darcy's law as a model to predict wicking time is recommended, but permeability of the type of paper selected for the device needs to be empirically understood prior to application in the model, until the concept of permeability can be characterized using theoretical parameters.

5.2 Recommendations

The following points are next steps and future works that were beyond the scope of this thesis:

- The interactions of flowing fluid in paper with reagents applied to the paper prior to wicking were not investigated in this study. It is imperative to understand the motion during imbibition of reagents that are placed on the paper.

- The SEM micrographs in this thesis demonstrated the complex structure of the paper fibre network. Impacts of fibre properties, such as elasticity and swelling, should be investigated to determine their impact on fluid flow through paper media.

- This thesis brought to light the need for a theoretical investigation on permeability of paper to determine an accurate mathematical model based on measureable and non-empirical variables. A successful investigation will lend significant prediction capacity not only for flow in paper-based microfluidic devices, but also a large variety of porous media.

- The model developed in this thesis is intended to be applied in the design of a highly effective paper-based microfluidic arsenic detection device. The flow behaviour predicted by this model will aid in the optimized selection for the location and quantity of reagents that will provide an accurate, reliable signal readout.

Bibliography

[1] W. H. Organization and UNICEF, “Progress on drinking water and sanitation 2013 update,” 2013.

[2] A. Pruss-Ustun, R. Bos, F. Gore, and J. Bartram, “Safe water, better health: costs, benefits, and sustainability of interventions to protect and promote health. 2008.,” 2008.

[3] U. Nations, “Millenium Development Goals and Beyond 2015: Goal 7 Fact Sheet,” 2013.

[4] W. A. Jury and V. J. H. J, “The emerging global water crisis: managing scarcity and conflict between water users,” *Adv. Agron.*, vol. 95, pp. 1–76, 2007.

[5] R. B. Johnston, S. Hanchett, and M. H. Khan, “The socio-economics of arsenic removal,” *Nat. Geosci.*, vol. 3, no. 1, pp. 2–3, Jan. 2010.

[6] a H. Smith, E. O. Lingas, and M. Rahman, “Contamination of drinking-water by arsenic in Bangladesh: a public health emergency.,” *Bull. World Health Organ.*, vol. 78, no. 9, pp. 1093–103, Jan. 2000.

[7] P. Atkins, M. Hassan, and C. Dunn, “Environmental irony: summoning death in Bangladesh,” *Environ. Plan. A*, vol. 39, no. 11, pp. 2699–2714, 2007.

[8] World Health Organization, “Arsenic in drinking-water: Background document for the development of WHO guidelines for drinking-water quality,” 2011.

[9] M. M. Karim, “Arsenic in groundwater and health problems in Bangladesh,” *Water Res.*, vol. 34, no. 1, pp. 304–310, Jan. 2000.

[10] D. Chakraborti, M. M. Rahman, B. Das, M. Murrill, S. Dey, S. Chandra Mukherjee, R. K. Dhar, B. K. Biswas, U. K. Chowdhury, S. Roy, S. Sorif, M. Selim, M. Rahman, and Q. Quamruzzaman, “Status of groundwater arsenic contamination in Bangladesh: a 14-year study report.,” *Water Res.*, vol. 44, no. 19, pp. 5789–802, Nov. 2010.

[11] B. K. Mandal and K. T. Suzuki, “Arsenic round the world: a review.,” *Talanta*, vol. 58, no. 1, pp. 201–35, Aug. 2002.

[12] UNICEF, “Arsenic Mitigation in Bangladesh,” 2010.

[13] C. F. Harvey, K. N. Ashfaque, W. Yu, a. B. M. Badruzzaman, M. A. Ali, P. M. Oates, H. a. Michael, R. B. Neumann, R. Beckie, S. Islam, and M. F. Ahmed, “Groundwater dynamics and arsenic contamination in Bangladesh,” *Chem. Geol.*, vol. 228, no. 1–3, pp. 112–136, Apr. 2006.

[14] M. M. Rahman, D. Mukherjee, M. K. Sengupta, U. K. Chowdhury, D. C. R. Lodh, S. Roy, M. Selim, Q. Quamruzzaman, A. H. Milton, S. M. Shahidullah, M. T. Rahman, and D. Chakraborti, “Effectiveness and reliability of arsenic field testing kits: are the million dollar screening projects effective or not?,” *Environ. Sci. Technol.*, vol. 36, no. 24, pp. 5385–94, Dec. 2002.

[15] M. Arora, M. Megharaj, and R. Naidu, “Arsenic testing field kits: some considerations and recommendations.,” *Environ. Geochem. Health*, vol. 31 Suppl 1, pp. 45–8, Apr. 2009.

[16] M. Jakariya, M. Vahter, M. Rahman, M. A. Wahed, S. K. Hore, P. Bhattacharya, G. Jacks, and L. A. Persson, “Screening of arsenic in tubewell water with field test kits: evaluation of the method from public health perspective.,” *Sci. Total Environ.*, vol. 379, no. 2–3, pp. 167–75, Jul. 2007.

[17] C. M. Steinmaus, C. M. George, D. a Kalman, and A. H. Smith, “Evaluation of two new arsenic field test kits capable of detecting arsenic water concentrations close to 10 microg/L.,” *Environ. Sci. Technol.*, vol. 40, no. 10, pp. 3362–6, May 2006.

[18] S. P. Pande, L. S. Deshpande, and S. N. Kaul, “Laboratory and field assessment of arsenic testing field kits in Bangladesh and West Bengal, India.,” *Environ. Monit. Assess.*, vol. 68, no. 1, pp. 1–18, Apr. 2001.

[19] P. Yager, T. Edwards, E. Fu, K. Helton, K. Nelson, M. R. Tam, and B. H. Weigl, “Microfluidic diagnostic technologies for global public health.,” *Nature*, vol. 442, no. 7101, pp. 412–8, Jul. 2006.

[20] H. Jayamohan, H. J. Sant, and B. K. Gale, “Microfluidic Diagnostics,” vol. 949, 2013.

[21] R. W. Peeling and D. Mabey, “Point-of-care tests for diagnosing infections in the developing world,” *Clin. Microbiol. Infect.*, vol. 16, no. Imci, pp. 1062–1069, 2010.

[22] H. Kettler, K. White, and S. Hawkes, “Mapping the landscape of diagnostics for sexually transmitted infections: Key findings and recommandations,” pp. 1–44, 2004.

[23] M. Rasi, “Permeability Properties of Paper,” University of Jyvaskyla, 2013.

[24] D. Schuchardt and J. Berg, “Liquid transport in composite cellulose-superabsorbent fiber network.,” *Wood Fiber Sci*, no. 23, pp. 342–357, 1990.

[25] R. J. ROBERTS, T. J. SENDEN, M. A. KNACKSTEDT, and M. B. LYNE, “Spreading of aqueous liquids in unsized papers is by film flow,” *J. pulp Pap. Sci.*, vol. 29, no. 4, pp. 123–131.

[26] M. Alava, M. Dubé, and M. Rost, “Imbibition in Disordered Media,” vol. 53, no. 2, p. 53, 2004.

[27] J. Hyvaluoma, P. Raiskinmäki, A. Jäsberg, A. Koponen, M. Kataja, and J. Timonen, “Simulation of liquid penetration in paper,” *Phys. Rev. E - Stat. Nonlinear, Soft Matter Phys.*, vol. 73, no. October 2005, pp. 1–8, 2006.

[28] R. Masoodi and K. M. Pillai, “Darcy’s Law-Based Model for Wicking in Paper-Like Swelling Porous Media,” *AIChE J.*, vol. 56, no. 9, pp. 2257–2267, 2010.

[29] S. Mendez, E. M. Fenton, G. R. Gallegos, D. N. Petsev, S. S. Sibbett, H. A. Stone, Z. Yi, and G. P. Lopez, “Imbibition in Porous Membranes of Complex Shape: Quasi-Stationary Flow in Thin Rectangular Segments,” *Langmuir*, vol. 26, no. 2, pp. 1380–1385, 29010.

[30] A. K. Yetisen, M. S. Akram, and C. R. Lowe, “Paper-based microfluidic point-of-care diagnostic devices.,” *Lab Chip*, vol. 13, no. 12, pp. 2210–51, Jun. 2013.

[31] E. Fu, S. A. Ramsey, P. Kauffman, B. Lutz, and P. Yager, “Transport in two-dimensional paper networks,” *Microfluid Nanofluidics*, vol. 10, no. 1, pp. 29–35, 2011.

[32] C. D. Chin, T. Laksanasopin, Y. K. Cheung, D. Steinmiller, V. Linder, H. Parsa, J. Wang, H. Moore, R. Rouse, G. Umviligihozo, E. Karita, L. Mwambarangwe, S. L. Braunstein, J. van de Wijgert, R. Sahabo, J. E. Justman, W. El-Sadr, and S. K. Sia, "Microfluidics-based diagnostics of infectious diseases in the developing world.," *Nat. Med.*, vol. 17, no. 8, pp. 1015–1019, 2011.

[33] M. M. Gong, B. D. MacDonald, T. V. Nguyen, K. Van Nguyen, and D. Sinton, "Lab-in-a-pen: a diagnostics format familiar to patients for low-resource settings.," *Lab Chip*, vol. 14, pp. 957–63, 2014.

[34] T. S. Park, W. Li, K. E. McCracken, and J.-Y. Yoon, "Smartphone quantifies Salmonella from paper microfluidics.," *Lab Chip*, vol. 13, pp. 4832–40, 2013.

[35] P. Nath, K. Arun, and N. Chanda, "A paper based micro fl uidic device for the detection of arsenic using a gold nanosensor †," *RSC Adv.*, vol. 4, pp. 59558–59561, 2014.

[36] E. Fu, B. Lutz, P. Kauffman, and P. Yager, "Controlled reagent transport in disposable 2D paper networks.," *Lab Chip*, vol. 10, no. December 2009, pp. 918–920, 2010.

[37] A. W. Martinez, S. T. Phillips, and G. M. Whitesides, "Three-dimensional microfluidic devices fabricated in layered paper and tape.," *Proc. Natl. Acad. Sci. U. S. A.*, vol. 105, no. 50, pp. 19606–11, Dec. 2008.

[38] M. Zimmermann, H. Schmid, and E. Delamarche, "Capillary pumps for autonomous capillary systems {," no. October 2006, pp. 119–125, 2007.

[39] H. Noh and S. T. Phillips, "Fluidic timers for time-dependent, point-of-care assays on paper.," *Anal. Chem.*, vol. 82, no. 19, pp. 8071–8, Oct. 2010.

[40] B. Lutz, T. Liang, E. Fu, S. Ramachandran, P. Kauffman, and P. Yager, "Dissolvable fluidic time delays for programming multi-step assays in instrument-free paper diagnostics.," *Lab Chip*, vol. 13, no. 14, pp. 2840–7, 2013.

[41] M. M. Gong, P. Zhang, B. D. MacDonald, and D. Sinton, "Nanoporous membranes enable concentration and transport in fully wet paper-based assays.," *Anal. Chem.*, vol. 86, pp. 8090–7, 2014.

[42] H. Bruus, *Theoretical Microfluidics*, 1st ed. New York: Oxford University Press, 2008.

[43] P. J. Pritchard, *Fox and McDonald's Introduction to Fluid Mechanics*, 8th ed. Hoboken, NJ: Wiley, 2011.

[44] T. Young, "An essay on the cohesion of fluids," *Philos. Trans. R. Soc. London*, pp. 65–87, 1805.

[45] P. Laplace, "On capillary attraction," *Suppl. to Tenth B. Mech. Celeste*, 1806.

[46] E. W. Washburn, "The dynamics of capillary flow," *Phys. Rev.*, vol. 17, pp. 273–283, 1921.

[47] R. Lenormand, C. Zarcone, and A. Sarr, "Mechanisms of the displacement of one fluid by another in a network of capillary ducts," *J. Fluid Mech.*, vol. 135, pp. 337–353, 1983.

[48] J. Songok, M. Tuominen, H. Teisala, J. Haapanen, J. Makela, J. Kuusipalo, and M. Toivakka, "Paper-Based Microfluidics: Fabrication Technique and Dynamics of Capillary-Driven Surface Flow," *ACS Appl. Mater. Interfaces*, vol. 6, pp. 20060–20066, 2014.

[49] H. Darcy, *The public fountains of the city of Dijon*. 1856.

[50] S. Whitaker, "Flow in Porous Media I," *Transp. Porous Media*, vol. 1, p. 3, 1986.

[51] E. Elizalde, R. Urteaga, and C. L. a. Berli, "Rational design of capillary-driven flows for paper-based microfluidics," *Lab Chip*, vol. 15, pp. 2173–2180, 2015.

[52] a. Koponen, D. Kandhai, E. Hellén, M. Alava, a. Hoekstra, M. Kataja, K. Niskanen, P. Sloot, and J. Timonen, "Permeability of Three-Dimensional Random Fiber Webs," *Phys. Rev. Lett.*, vol. 80, no. 4, pp. 716–719, 1998.

[53] F. Dullien, *Porous Media: Fluid Transport and Pore Structure*. San Diesgo: Academic Press, 1992.

[54] GE Life Sciences, "Typical Properties of Whatman Filter Papers." [Online]. Available: www.gelifesciences.com.

[55] Advantec, “Specialty Products: Blotting and Chromatography Paper.” [Online]. Available: www.advantecmfs.com.

[56] H. G. Cassidy, “Investigation of Paper Chromatography,” *Anal. Chem.*, vol. 24, no. 9, pp. 1415–1421, 1952.

[57] H. Noh and S. T. Phillips, “Metering the capillary-driven flow of fluids in paper-based microfluidic devices.,” *Anal. Chem.*, vol. 82, no. 10, pp. 4181–7, May 2010.

[58] X. Li, D. R. Ballerini, and W. Shen, “A perspective on paper-based microfluidics: Current status and future trends.,” *Biomicrofluidics*, vol. 6, no. 1, pp. 11301–1130113, Mar. 2012.

[59] A. Böhm, F. Carstens, C. Trieb, S. Schabel, and M. Biesalski, “Engineering microfluidic papers: effect of fiber source and paper sheet properties on capillary-driven fluid flow,” *Microfluid. Nanofluidics*, Jan. 2014.